



RESEARCH ARTICLE

10.1029/2019JF005287

This article is a companion to Barnhart et al. (2020b, 2020c), <https://doi.org/10.1029/2018JF004961> and <https://doi.org/10.1029/2018JF004963>.

Key Points:

- We provide a compilation of parameter ranges for mature geomorphic transport laws in terrestrial geomorphology
- A simple hydrological model connects changes in the precipitation distribution with erodibility coefficients
- Common challenges include incomparable units and mismatch between observation and simulation timescales

Correspondence to:

K. R. Barnhart,
katherine.barnhart@colorado.edu

Citation:

Barnhart, K. R., Tucker, G. E., Doty, S. G., Shobe, C. M., Glade, R. C., Rossi, M. W., & Hill, M. C. (2020). Inverting topography for landscape evolution model process representation: 3. Determining parameter ranges for select mature geomorphic transport laws and connecting changes in fluvial erodibility to changes in climate. *Journal of Geophysical Research: Earth Surface*, 125, e2019JF005287. <https://doi.org/10.1029/2019JF005287>

Received 2 AUG 2019

Accepted 11 FEB 2020

Accepted article online 18 FEB 2020

Inverting Topography for Landscape Evolution Model Process Representation: 3. Determining Parameter Ranges for Select Mature Geomorphic Transport Laws and Connecting Changes in Fluvial Erodibility to Changes in Climate

Katherine R. Barnhart^{1,2} , Gregory E. Tucker^{1,2} , Sandra G. Doty³, Charles M. Shobe^{1,2,4} , Rachel C. Glade^{1,5,6} , Matthew W. Rossi⁷ , and Mary C. Hill⁸

¹Cooperative Institute for Research in Environmental Sciences, University of Colorado Boulder, Boulder, CO, USA, ²Department of Geological Sciences, University of Colorado Boulder, Boulder, CO, USA, ³Denver, CO, USA, ⁴Helmholtz Centre Potsdam, GFZ German Research Centre for Geosciences, Potsdam, Germany, ⁵Institute for Arctic and Alpine Research, University of Colorado Boulder, Boulder, CO, USA, ⁶Earth and Environmental Sciences Division, Los Alamos National Laboratory, Los Alamos, NM, USA, ⁷Earth Lab, University of Colorado Boulder, Boulder, CO, USA, ⁸Department of Geology, University of Kansas, Lawrence, KS, USA

Abstract We review select mature geomorphic transport laws for use in temperate ridge and valley landscapes and compile parameter estimates for use in applications. This work is motivated by a case study of sensitivity analysis, calibration, validation, multimodel comparison, and prediction under uncertainty, which required bounding values for parameter ranges. Considered geomorphic transport formulae span hillslope sediment transport, soil production, and erosion by surface water. We compile or derive estimates for the parameters in these transport formulae. Additionally, we address a common challenge—connecting changes in precipitation distribution to changes in effective erodibility—by using a simple hydrologic model and a method to estimate precipitation distribution parameters using commonly available data. While some parameters are reasonably well constrained, others span orders of magnitude. Some, such as soil infiltration capacity, have a direct physical meaning but are challenging to measure on geologically relevant timescales. Through the process of compiling these ranges we identify common challenges in parameter determination. The issue of comparable units derives from considering an exponent as an empirically inferred coefficient rather than as an expression of a fundamental relationship. The issue of appropriate timescales derives from the mismatch between human measurement and geologic timescales. This contribution thus serves both as a practical compilation for applications and as a synthesis of outstanding challenges in parameter selection for geomorphic transport laws.

1. Introduction

The surface of Earth is modified by an array of physical and chemical processes that dynamically change its properties and shape. Major classes of the processes that act on rock and soil are (i) changes in physical properties such as size, mechanical strength, or density; (ii) the horizontal and vertical motion of material by entrainment, advection, and disentrainment in a transporting fluid such as ice, snow, water, or wind; (iii) gravity-driven motion of material in the absence of such a fluid (e.g., rockfall or landslide).

A mechanistic (or at least mechanistically inspired) understanding of these processes is necessary for applications as diverse as interpreting geologic records of faulting (Andrews & Hanks, 1985; Andrews & Bucknam, 1987; Hanks, 2000; Pelletier et al., 2006), understanding the evolution of land surface form (e.g., Rosenbloom & Anderson, 1994), and addressing core questions in geomorphology such as the controls on relief and drainage density. The rate of change of Earth's surface is slow relative to a human lifetime; thus, opportunities to test alternative hypotheses about processes that act on geomorphic timescales in natural environments (rather than in a scaled laboratory setting or a highly-instrumented short-term natural setting) are limited to well-constrained natural experiments (Tucker, 2009).

Formal testing of alternative hypotheses in process geomorphology requires a mathematical expression that describes a process in terms of controlling independent variables (such as temperature, land surface slope, surface water discharge, or upstream contributing area). Constructing such a statement first requires a conceptual-mechanistic model of the process, typically grounded in observation and empirical evidence. This conceptual-mechanistic model is then represented mathematically. For example, the commonly used mathematical model for transport of mobile material by slope-dependent processes originates with observations by Gilbert (1877) and Davis (1892) and was formalized mathematically by Culling (1960).

In the slope-dependent transport example, the mathematical representation takes the form of a mass flux law. Other geomorphic process models take the form of a stability criterion; an example is the Mohr-Coulomb friction threshold for mass failure initiation. A final class of mathematical representation includes so-called “rule-based” models—heavily informed by physical principles and mass conservation, but not directly mechanistic. An example of this latter class would be the rule for distributing landslide runoff used by Densmore et al. (1998). Also in this category are cellular automaton models that use physical meaningful parameters (e.g., Narteau et al., 2009; Tucker et al., 2018).

Collectively, mathematical models that describe erosion or mass flux by one or more physical processes are referred to as *geomorphic transport laws* (GTLs; Dietrich et al., 2003). These authors further describe GTLs as mathematical models that can be “observed, parameterized, and verified by field or laboratory experiment.” Thus, GTLs may be entirely empirical or be grounded in mechanistic theory. The primary concern of our contribution is to summarize estimates of parameter values for those GTLs that describe hillslope and valley topography and for which sufficient efforts relating to parameter estimation have occurred to justify such a review.

Mathematical and numerical models of Earth surface dynamics combine one or more of these mathematical models with initial and boundary conditions to simulate real or synthetic domains, either analytically or numerically. GTLs are used in individual or coupled sets of 1-D numerical models of hillslope and channel profiles, in 2.5-D numerical models, and in analytical solutions for simplified (e.g., equilibrium) 1-D profile forms. When model analysis methods (such as sensitivity analysis and calibration) are applied to Earth surface dynamics problems, reasonable estimates and/or ranges for parameter values are necessary.

This work extended from a motivating case study described in section 2.1 that required estimates of parameter ranges for sensitivity analysis, calibration, validation, and prediction under uncertainty. The effort confronted a common challenge in applying GTLs to the geologic past and future: representing changes in climate in terms of changes in an effective rate coefficient for erosion by surface water. Thus, after describing parameter estimates in sections 3–5, we present an approach in section 6 for linking changes in precipitation through geologic time with fluvial erodibility coefficients. Our analysis of precipitation distributions is focused at a single location and focuses on future changes in climate. However, the general approach is portable to other locations and timescales. We end by discussing the common challenges in parameter estimation for GTLs that our review identified.

2. Approach and Scope

Here we focus on the GTLs for processes that shape hillslope and valley topography on timescales greater than 10^3 yr. Specifically we focus on the evolution of hillslopes under gravity-driven processes and the erosion of geological materials by flowing surface water.

2.1. Motivating Case Study

This focus originates from a motivating case study in postglacial landscape evolution in western New York state, USA. To provide context for the choice of processes and space and timescales addressed in this review, we provide here a brief summary of the original motivating case study; the study and its objectives are described in two companion papers (Barnhart et al., 2020b, 2020c). The study site includes two small (several square kilometer) watersheds that are underlain by Devonian shale bedrock. The most recent glaciation left behind thick glacial deposits in the main valley to which both watersheds drain, and since deglaciation at ~ 13 ka, the major streams have incised up to ~ 50 m into these deposits (Fakundiny, 1985; Wilson & Young, 2018). The study area provides an example of a practical application of landscape evolution modeling, because the storage of radiological waste material at the site creates a need for future forecasts of long-term erosion. This need motivates a model testing and calibration exercise based on the inferred patterns of

landscape evolution following the most recent retreat of the Laurentide ice from the area. The two companion papers describe the site in greater detail, and present a sensitivity analysis, calibration, and validation of 37 alternative landscape evolution models in order to identify usable models for erosion forecasts at the site.

2.2. Considered Geomorphic Transport Laws

Many GTLs have been articulated for the evolution of temperate hillslope and valley topography on these time and space scales. Of these GTLs, most remain speculative. Only a small number of proposed GTLs have been subject to sufficient study such that multiple estimates of their parameters have been made on the relevant timescales. We will refer to this subset as “mature” GTLs. Debris flow erosion, lateral erosion of channel banks, and channel width adjustment are examples of relevant processes that presently lack mature GTLs: the processes are within the domain scope we define, but either has a mathematical form that is still in development (e.g., Langston & Tucker, 2018, for lateral erosion) or has few to no parameter estimates. The absence of many processes from this set of “mature” GTLs motivates future work and is discussed at the end of this contribution. We further restrict our scope by considering only mass flux and erosion-type process expressions, and neglecting stability criterion expressions.

The studies we review derive parameter estimates from a wide range of timescales. For example, two studies that address incision by water in well-constrained natural experiments use timescales of ~ 100 yr (Whipple, Snyder, et al., 2000) and 20 Ma (van der Beek & Bishop, 2003). While the considered timescales span multiple orders of magnitude, the key shared quality of both studies is that they integrate over multiple morphology-forming erosion events. Nonetheless, the compiled parameter ranges should be considered in light of what are sometimes vastly different timescales of estimation.

We note that a long-standing goal of the scientific community is a set of mechanistically derived statements for erosion and mass flux that are applicable across a wide range of time and space scales, lithologies, and field sites. However, most of the mature GTLs do not yet meet these criteria. As we discuss further in section 5.1.2, one common challenge is a lack of data: the scientific community may have a reasonable mechanistic understanding of a given process (such as evapotranspiration) yet lack information about key inputs or state variables (such as wind speed or land surface temperature) that would be needed to apply that mechanistic theory on long timescales. Another common challenge is computational; for example, even if one had perfect knowledge of the past weather, topography, and materials, it would still not be feasible (given present technology) to compute the eddy scale, 3-D turbulent hydraulics of an evolving stream network over thousands of years. To be useful, a GTL must be practical—both in terms of data and model state variable requirements and computational feasibility. Hence, our focus here is on reasonably mature GTLs that are practical in both of these senses, with an eye toward applications at the spatial scale of several square kilometers or larger, and the timescale of millennia to tens of millennia (which are the applicable space and timescales of the motivating application discussed in section 2.1).

Moreover, our choice of GTLs to review should not be taken to imply that any of them are the last or best word on the subject. Rather, it is important to bear in mind that today's generation of mature and practical GTLs are provisional in nature, having some basis in process theory and some explanatory power, but also necessarily simplified, and not universally applicable. Our intention here is simply to identify parameter ranges for several practical and widely used GTLs, to support cases in which a practitioner has decided that using one or more of them is reasonable for their purposes.

2.3. Conservation of Mass Framework

Our consideration of GTLs is grounded in a general conservation of mass framework. We present governing equations for two cases: gravitational transport on hillslopes (equations (1)–(3)) and erosion by channelized and unchannelized surface water (equation (5)). When describing the case of gravitational transport we consider the following variables: the elevation of the topographic surface η , the elevation of the bedrock surface η_b , and the thickness of a mobile regolith or soil layer H , such that

$$\eta = \eta_b + H. \quad (1)$$

The bedrock elevation is modified through the production of mobile material at a rate P_s (the thickness of added mobile material per time), and by rock uplift relative to base level at a rate $B_c(x, y, t)$:

$$\frac{\partial \eta_b}{\partial t} = B_c(x, y, t) - P_s. \quad (2)$$

Here x and y are the plan view dimensions and t is the time dimension. H evolves as

$$\frac{\partial H}{\partial t} = \frac{\rho_s}{\rho_r} P_s - \nabla \cdot \mathbf{q}_h, \quad (3)$$

where ρ_s/ρ_r represents the density contrast between soil and rock, and \mathbf{q}_h is the sediment flux per unit width due to gravity driven processes. The bold font in \mathbf{q}_h (and other symbols) indicates that this is a vector quantity; when written as q_h or $|\mathbf{q}_h|$ it represents magnitude without regard to direction. Note also that in this contribution we will not introduce dimensions in the text, and will only present units alongside a specific value. The Notation section provides a compilation of all symbols, including the dimensions associated with each quantity.

Two sets of assumptions result in two alternate forms for using equations (1)–(3). If soil thickness H is considered to have a potential influence on landform evolution, then a formal representation of H is required, and \mathbf{q}_h may depend on H . In contrast, if one assumes that there is an unlimited thickness of mobile material, then the mass conservation equation reduces to

$$\frac{\partial \eta}{\partial t} = -\nabla \cdot \mathbf{q}_h. \quad (4)$$

The above simplification is sometimes referred to as the transport-limited assumption, because it implies that hillslope evolution is dictated by the transport rate field (Carson & Kirkby, 1972).

When considering erosion by surface water we can write the time rate of change of land surface elevation as

$$\frac{\partial \eta}{\partial t} = B_c(x, y, t) - E, \quad (5)$$

where E represents the rate of erosion (if positive) or deposition (if negative) resulting from surface water processes.

There are a few approaches to treating E , each of which represents an alternative GTL. First, consider a case in which the detachment of material by flowing water is the limiting process in modifying the topography and the rate of detachment does not depend on the sediment flux carried by the flow. This case is often called *detachment limited* (Howard, 1994). A variant of this case is one in which detachment of material is the limiting process and its rate depends on the sediment flux. Second, in the transport-limited case, it is the transport of material and not its detachment that limits the modification of the topography. The two end-member approaches to E make no assumption about the type of material that is detached or transported; field studies have shown, for example, that disaggregated material may behave consistently with detachment-limited theory (e.g., Hobbey et al., 2011) whereas rock erosion may behave in agreement with transport-limited theory (Valla et al., 2010). Note also that we have not distinguished between erosion by channelized or unchannelized flow (discussed further in section 5).

As described above, mature GTLs are proposed expressions for E , \mathbf{q}_h , and P_s that have multiple parameter estimates on relevant timescales. A summary of the expressions we consider is presented in Table 1. Each requires one or more parameters, and the remainder of this contribution focuses on identifying a reasonable basis for these parameters. In the following sections, we provide background for the GTLs in question. In providing this background we do not extensively review the derivation and application of each GTL. Instead, we focus on reviewing the literature in which parameter estimates are obtained.

2.4. Precipitation and Discharge

Because E implicitly describes the flow of surface water, we will not completely neglect the surface water discharge, Q . However, a full review of surface and subsurface hydrologic models and the parameters therein is beyond the scope of this contribution. Instead, in section 6 we will discuss and estimate parameters that describe the precipitation distribution as well as the infiltration capacity. This portion of the text has two motivations. First, the stochastic hydrology models in the companion papers require estimates of these parameters (Barnhart et al., 2020b, 2020c). Second, compilation of modern and future values of these parameters allows us to address a common challenge in applying geomorphological models on geologic timescales: the link between climate—as represented by a precipitation distribution—and the coefficients used to calculate E .

Table 1
Considered Geomorphic Transport Rule Formulae

Process	Name	Equation and Equation Number	Parameters	Key Reference(s)
Gravitational transport	Linear	$\mathbf{q}_h = -D\nabla\eta$ (6)	D	Culling (1963)
	Nonlinear	$\mathbf{q}_h = -D\nabla\eta \left[1 + \sum_{i=1}^N \left(\frac{ \nabla\eta }{S_c} \right)^{2i} \right]$ (7)	D, S_c, N	Andrews and Bucknam (1987), Roering et al. (1999), Ganti et al. (2012)
Soil production	Exponential	$P_s = P_0 \exp\left(-\frac{H}{H_s}\right)$ (8)	P_0, H_s	Armstrong (1976)
Surface water erosion	Vertical detachment rate	$E = \max(KA^m S^n - \omega_c, 0)$ (9)	K, m, n, ω_c	Howard (1994), Whipple and Tucker (1999)
	Modification of topography due to gradients in sediment carrying capacity	$E = \frac{1}{1-\phi} \nabla \cdot \mathbf{q}_s$ (10)	$K_t, m_t, n_t, \omega_{t,c}$	Many equations exist for \mathbf{q}_s . They are often simplified to consider only the stream-wise direction q_s . See text for discussion
		$= \frac{1}{1-\phi} \frac{1}{W} \frac{d(K_t A^{m_t} S^{n_t} - \omega_{t,c})}{dx}$ (11)		

Note. Symbols are defined as they are introduced in the text as well as in the Notation and Table 2.

Whether the details of precipitation itself, or the basin hydrology characteristics that convert precipitation into discharge, manifest in a distinct landscape morphology is an open question (e.g., Huang & Niemann, 2006, 2008). Nonetheless, we know that both sediment transport and erosion depend on surface water discharge, and hence should be influenced by changes in precipitation amount and/or frequency over time. Because the efficiency of long-term water erosion and/or sediment transport is often represented by a lumped coefficient, it is useful to have a method by which changes in precipitation magnitude and frequency can be expressed in terms of changes in this rate parameter. In section 6, we propose such a method.

One might argue that a better approach is to formally represent precipitation, basin hydrology, and thus discharge in models that incorporate GTLs. However, such an approach would add considerable complexity by requiring additional parameters that are challenging to constrain on geological timescales. We discuss this issue further in section 7.5.

2.5. Distinction Between Geomorphic Transport Laws and Numerical Implementation

We focus on the form and parameters of mature GTLs rather than on how those GTLs might be implemented in a 2-D numerical landscape evolution model, or in a 1-D numerical model of channel or hillslope profile evolution. To this end we have been intentionally vague regarding whether a specific implementation using GTLs considers a domain that is 1-D or 2-D. We have also intentionally not described use of mathematical models or GTLs using the term “landscape evolution model” (LEM). This is because our intent is to focus on estimates of parameters used in the general application of GTLs, rather than their specific numerical implementations either in 1-D profile models or in 2-D LEMs (for a review of LEMs, see Bishop, 2007; Coulthard, 2001; Codilean et al., 2006; Chen et al., 2014; Martin & Church, 2004; Pazzaglia, 2003; Pelletier, 2013; Temme et al., 2013; Tucker & Hancock, 2010; Valters, 2016; Willgoose, 2005; Willgoose & Hancock, 2011).

3. Hillslope Sediment Transport

Gravitational hillslope sediment transport is typically treated as a diffusion-like process. Table 1 describes two different GTLs for hillslope sediment transport: linear (equation (6), Culling, 1963) and nonlinear (equation (7), Andrews & Bucknam, 1987; Roering et al., 1999, 2001; Roering, 2008). Both laws use a soil creep rate coefficient D ; the nonlinear version adds a critical slope gradient S_c . While the mathematical forms of equations (6) and (7) differ, the parameter D has the same meaning in both equations, as the two are equivalent when the local slope $\nabla\eta$ is much greater than S_c .

3.1. Soil Creep Rate Coefficient, D

The soil creep rate coefficient D represents the efficiency with which soil is transported downslope for a given local topographic gradient. It has dimensions of $[L^2/T]$, and estimates in the literature are often reported in

square meters per year, square centimeters per year, or square meters per thousand years. It appears in the equations describing soil flux (equations (6) and (7)).

Because many models assume that hillslope evolution is a diffusion-like process, this efficiency term is often referred to as *hillslope diffusivity*. A variety of techniques have been used to estimate values of D in different settings. These methods range from fitting theoretical hillslope profiles to degraded scarps (e.g., Hanks et al., 1984; Nash, 1980; Pelletier et al., 2006) to the use of cosmogenic radionuclide measurements in conjunction with mass-balance models (e.g., McKean et al., 1993; Small et al., 1999). The most recent comprehensive list of published estimates is found in Richardson et al. (2019). Most estimates of D fall in the range 10^{-4} to 10^{-2} m^2yr^{-1} and vary with mean annual precipitation, aridity index, and vegetation type (Richardson et al., 2019).

One of the highest published estimates comes from a study which uses a model with linear diffusion to estimate D for Wasatch fault facets ($D = 0.13$ m^2yr^{-1} ; Petit et al., 2009). We discuss the interpretation of this result in section 7.4.

3.2. Threshold Slope Gradient, S_c

Field and laboratory experimental work suggest a nonlinear relationship between slope angle and the rate of downslope soil creep (e.g., Roering et al., 1999, 2001). A common representation of this relation is the Andrews-Bucknam equation:

$$\mathbf{q}_s = -D\nabla\eta \left[\frac{1}{1 - \left(\frac{|\nabla\eta|}{S_c}\right)^2} \right], \quad (12)$$

where $\nabla\eta$ is slope gradient and S_c is a critical gradient. One obvious drawback of this formulation is that it is undefined for $|\nabla\eta| \geq S_c$. An alternative approach, suggested by Ganti et al. (2012), is to use the leading terms in a truncated Taylor expansion of the Andrews-Bucknam equation using N terms. Here, we adopt this as a useful generalization; the truncated series form, which equates to a sum of N odd-numbered powers of $|\nabla\eta|/S_c$, is given in Table 1 as equation (7). As $N \rightarrow \infty$ equation (7) converges to equation (12)

The nonlinear hillslope transport GTL includes a “critical slope” parameter, S_c . This parameter represents the gradient near which the downslope soil flux becomes significantly greater than a simple linear formulation between gradient and flux would predict. Equation (7) represents the Taylor series expansion of the Andrews-Bucknam equation (Andrews & Bucknam, 1987). The equivalent parameter in the more familiar Andrews-Bucknam equation represents the gradient at which soil flux becomes infinite; the equation is undefined for gradients steeper than this value and hence equation (7) is preferred.

Published estimates of S_c in the Andrews-Bucknam equation come from either sand-pile experiments or terrain analysis. Roering et al. (2001) report values of $S_c = 0.6$ from sand pile experiments. One approach to terrain analysis uses a slope versus curvature plot to infer a value for S_c . Using this method, Roering et al. (1999) report values of $S_c = 1.25 \pm 0.1$ for the Oregon Coast Range and Roering et al. (2007) report values of $S_c = 1.2 \pm 0.4$ for Gabilan Mesa, California. A second terrain analysis approach uses a hillslope length versus relief plot to infer S_c (Grieve et al., 2016). This method yields values of $S_c = 0.57$ for Coweeta, North Carolina; $S_c = 0.79$ for the Oregon Coast range; $S_c = 0.8$ for Gabilan Mesa, California; and $S_c = 0.7254 \pm 0.0015$ (Grieve et al., 2016, their Figure 10).

These two topographic analysis methods produce different values for the same sites. As discussed by Grieve, Mudd, and Hurst (2016) and Grieve, Mudd, Hurst, and Milodowski (2016), the estimate from hillslope length-versus-relief plots reflects an average S_c value, whereas estimates from slope-versus-curvature plots constrain the upper bound of S_c . Table 2 lists a broad range for S_c of 0.6 to 1.4.

4. Soil Production

Next we discuss parameters that describe the rate of soil production. There are many processes that contribute to soil formation, but to date the only GTL that has a substantial body of field evidence describes the relationship between soil production and soil depth.

We review four forms of the relationship between soil production and soil depth. Young (1963) and Culling (1965) both suggested a hyperbolic relationship in which soil production goes as $\sim 1/H$. Armstrong (1976)

Table 2
Compiled Parameter Names, Ranges, and Units

Symbol	Description	Units	Lower bound	Upper bound
Gravitational transport				
D	soil creep coefficient	m^2yr^{-1}	10^{-7}	10^{-1}
S_c	critical slope gradient	m.m^{-1}	0.6	1.4
Soil production				
P_0	maximum soil production rate	m.yr^{-1}	10^{-6}	10^{-3}
H_s	soil production depth scale	m	0.2	0.7
Surface water erosion				
m	detachment-limited drainage area exponent	-	See section 5.4	
m_t	transport-limited drainage area exponent	-	See section 5.4	
n	detachment-limited slope exponent	-	See section 5.4	
n_t	transport-limited slope exponent	-	See section 5.4	
K	detachment-limited stream power erosion coefficient	$\text{m}^{(1-2m)}\text{yr}^{-1}$	10^{-15}	10^0
K_t	transport-limited stream power erosion coefficient	$\text{m}^{(3-2m_t)}\text{yr}^{-1}$	1×10^{-8}	1×10^{-3}
ω_c	erosion threshold	m.yr^{-1}	0.0	see text

Note. All symbols are also defined with dimensions in the Notation section.

suggested a form in which the rate of soil production decreases exponentially with increasing soil thickness. A third form is the “humped” expression in which soil production reaches a maximum under some thickness of soil and then decreases with further increases in soil thickness (described by Cox, 1980, as “Kirkby’s hypothesis”). The final proposed form is a power law expression based on percolation theory (Hunt, 2015; Hunt & Ghanbarian, 2016). The primary parameter used in this expression is based on the net infiltration rate. With the exception of the final, power-law form, no proposed forms are theoretically linked with a mechanism of soil production.

The core observations that constrain the parameters used by or distinguish between any of the four forms described above are the same: observations of soil thicknesses and cosmogenic radionuclide-derived ages. In the remainder of this section we only discuss parameter estimates associated with the exponential form because it has received the most scrutiny in the literature.

Evidence for a humped function comes from observations of cosmogenic radionuclide-based soil-production-functions from select sites (e.g., Heimsath et al., 2009). It has more parameters than the two-parameter exponential expression: the form proposed by Kirkby and described by Cox (1980) has five parameters while that used by Anderson (2002) has four parameters. We do not consider the humped form here because of the increased number of parameters required to describe it and the smaller number of studies that provide empirical support for it.

Hunt (2015) compares the exponential-decay and power-law based expressions and finds nearly equivalent regression performance (exponential decay $R^2=0.46$; power law $R^2=0.48$). He argues that because the fitted power is close to the result predicted by percolation theory, the power-law form should be preferred. While this expression shows promising performance, we do not consider it because it has only recently been proposed and is not commonly considered.

4.1. Maximum Soil Production Rate, P_0

Several studies have used cosmogenic radionuclide analysis to estimate the maximum soil production rates, which corresponds to the erosion model parameter P_0 . Stockmann et al. (2014) compiled field-estimated rates and found that they range from 7×10^{-6} to 2×10^{-3} m.yr^{-1} . The lowest rate derives from a rocky, high alpine environment, and the highest in a temperate climate at a site experiencing rapid rock uplift. Based on these studies, a reasonable range for calibration and sensitivity analysis, rounding to orders of magnitude, is 10^{-6} to 10^{-3} m.yr^{-1} .

4.2. Soil Production Characteristic Depth Scale, H_s

Studies have shown the soil production decay depth to be approximately 0.5 m in a number of sites around the world (Heimsath et al., 1997, 1999, 2001; Heimsath et al., 2001; Rosenbloom & Anderson, 1994). Here a bounding range of 0.2–0.7 m is recommended.

5. Erosion by Surface Water

Next, we consider two GTLs that treat erosion by flowing water. We will not distinguish between erosion by flowing water in unchannelized areas (e.g., overland flow on hillslopes) and in channels. While we will use GTLs derived for channelized flow, we note that similar discharge slope, area slope, and length slope forms have been used to address runoff erosion on hillslopes (Flanagan et al., 2001; Kirkby, 1969, 1994; Kirkby et al., 1998; Kirkby & Cox, 1995; Prosser & Rustomji, 2000, 1995).

Equations (9) and (10) present mature GTLs for the vertical detachment of material by surface water and modification of topography due to gradients in sediment carrying capacity (Howard, 1980; Howard & Kerby, 1983; Howard et al., 1994; Snow & Slingerland, 1987; Willgoose et al., 1991a; Whipple & Tucker, 1999; Whipple, 2004). We consider only vertical erosion, because theory for lateral erosion and valley widening remains a frontier (e.g., Hancock & Anderson, 2002; Langston & Tucker, 2018).

5.1. Detachment of Material by Flowing Water and the Parameter K

5.1.1. Theoretical Background

The form of the governing equation for detachment has been extensively discussed in the literature (e.g., Howard & Kerby, 1983; Howard et al., 1994; Whipple & Tucker, 1999). The formulas derive from a statement that erosion is related to excess shear stress or stream power per unit area of channel bed (unit stream power):

$$E = k_{e1} (\tau - \tau_c)^a \quad (13)$$

for the shear stress case, or

$$E = k_{e2} (\tau U - \tau_c U_c^*)^a \quad (14)$$

for the unit stream power case. Here k_{e1} and k_{e2} are generic erosion efficiency constants, U is the water velocity, U_c^* is the critical shear velocity, τ is the bed shear stress, and τ_c is the threshold shear stress below which no detachment occurs. The exponent a has been proposed to reflect the physical process by which particles are detached from the channel bed (Whipple & Tucker, 1999; Whipple, Hancock, et al., 2000). An alternative form that has analytical advantages results from distributing the exponent to each of the terms inside of the parenthesis (Tucker, 2004, his equation (7)). For example, equation (14) becomes

$$E \sim k_{e2} \left[(\tau U)^a - (\tau_c U_c^*)^a \right] \quad (15)$$

Transforming equations (13) or (14) into the form presented in equation (9) requires a statement of conservation of mass for water, conservation of momentum, a channel hydraulic geometry that relates Q to channel width, W , and a friction relationship to calculate τ (e.g., Howard, 1994; Tucker & Slingerland, 1997).

On the one hand, we might expect a more robust empirical relationship between E and shear stress or stream power because these quantities represent the channel hydraulics that are fundamental to the erosion process. However, in many applications, especially those operating in geologic time, it is not possible to know the channel hydraulics (and thus shear stress or stream power) with much precision. In such applications, it is common to assume an “effective” value of discharge—one whose geomorphic effect is equivalent to that of a natural sequence of flows over a long time period. The effective discharge, in turn, is assumed to scale with drainage area (A). Using drainage area as a proxy for stream discharge represents a considerable simplification to drainage basin hydrology and is not appropriate for all applications, but it makes a convenient practical choice for many long-term applications because drainage area can be calculated directly from topography.

Shear stress or stream power are often calculated based on A using a basin hydrology and channel hydraulic scaling relationship. The basin hydrology scaling is given as

$$Q = k_q A^{c_q} \quad (16)$$

where k_q and c_q are positive constants determined by fitting empirical data for basin characteristics (Gleason, 2015; Hack, 1957; Slingerland et al., 1994). Here Q is the geomorphically effective discharge (Wolman & Miller, 1960). When $c_q = 1$, then k_q can be thought of as an “effective runoff rate.” Similarly, channel width can be represented as a function of discharge using the hydraulic geometry relation:

$$W = k_w Q^{c_w} \quad (17)$$

where k_w and c_w are positive constants (Leopold & Maddock, 1953; Yalin, 1992). In our compilation we will focus on estimates made as a function of A .

Choices relating to the value of a , the $Q \sim W$ scaling, and the choice of friction relationship used (e.g., Chezy, Darcy-Weisbach, Manning), all manifest in different values for m and n , the area exponent, and the slope exponent in equation (9). Whipple and Tucker (1999) provide a derivation of these equations including a description of how scaling coefficients and exponents all combine into the values for K , m , and n (their equations (8)–(10)). The choice of exponent values is discussed further in section 5.4. In applications for which it is necessary to track the fate of the detached sediment (e.g., for deposition in an alluvial fan), one approach is to calculate the cumulative sediment flux using the upstream integral of E .

Equation (9) is commonly called the stream power incision model and it represents a considerable simplification of water erosion. It is widely used because its two state variables, S and A , can be calculated directly from topographic data, and because it has a small number of parameters. A wide variety of literature has explored its successes and failures (see review by Lague, 2013). It is generally regarded as a formulation for long timescales, over which many erosion events occur. The stream power model can account for primary features such as concave-upward channel profiles and migrating knickzones. One would not expect it to perform well on single-event timescales (see, for example, such a test in Beer & Turowski, 2015). Tests of this and other fluvial GTLs require well-constrained natural experiments (Tucker, 2009). These usually require the reconstruction of initial (paleo) landscapes or river long profiles, and typically attempt to invert for various unknown quantities by simulating long profile evolution from the past to the present (Attal et al., 2011, 2008; Hobley et al., 2011; Tomkin et al., 2003; van der Beek & Bishop, 2003; Valla et al., 2010; Whipple, Snyder, et al., 2000).

Equation (9) neither captures all observations nor represents a complete mechanistic understanding of erosion by flowing water (the achievement of which remains a work in progress in the scientific community), but it does represent a practical choice for certain applications in long-term landform evolution. For those applications, practitioners need parameter constraints—and hence one focus of this work is to review available estimates for those parameters.

5.1.2. Sediment Flux Dependent Incision

Equation (9) does not explicitly describe a dependence of the rate of erosion on the flux of sediment in the river, q_s , relative to its sediment carrying capacity q_c . Yet sediment can influence stream incision in two ways: providing tools with which to erode the bed (Foley, 1980; Sklar & Dietrich, 1998, 2004), and shielding the sub-sediment bed material from hydraulic stress and sediment impacts (Gilbert, 1877).

Laboratory efforts have worked to document and characterize both “tools” and “cover” effects (Chatanantavet & Parker, 2008; Finnegan et al., 2007; Johnson & Whipple, 2007, 2010; Shepherd, 1972; Sklar & Dietrich, 2001; Shepherd & Schumm, 1974). Theoretical efforts to describe both effects originated with Sklar and Dietrich (2004), were extended by Lamb, Dietrich, and Sklar (2008) to include the effects of suspended load, and reparameterized using dedicated experimental data by Auel et al. (2017). Field studies focused on event and seasonal timescales have found evidence for both effects (e.g., Beer & Turowski, 2015; Inoue et al., 2014; Johnson et al., 2010; Turowski & Rickenmann, 2009; Turowski et al., 2008; Yanites et al., 2011). Over longer timescales evidence for sediment flux dependence on incision comes from analysis of river incision patterns (Cowie et al., 2008; Finnegan et al., 2008; Hobley et al., 2011; Johnson et al., 2009). Finally, modeling studies have explored how these effects manifest in real and synthetic landscapes (e.g., Gasparini et al., 2006; Hobley et al., 2011; Sklar & Dietrich, 2006; Whipple & Tucker, 2002).

The extensive mechanistic theory (Sklar & Dietrich, 2004; Lamb, Dietrich, & Sklar, 2008; Turowski et al., 2007) and validation by field and laboratory measurements provides evidence and support for a more complex GTL than equation (9) that incorporates sediment flux dependence. However, field studies document complex relationships between the functional form of sediment flux dependence, within-event discharge

and sediment supply variability (e.g., Turowski & Rickenmann, 2009). This evidence illustrates the difficulty of implementing sediment flux dependence on geologic timescales. Modeling studies which incorporate sediment flux dependence typically use a function $f(q_s/q_c)$ that is bounded between 0 and 1 to represent the effect of sediment flux dependence (e.g., Gasparini et al., 2006; Hobbey et al., 2011). How to parameterize $f(q_s/q_c)$ for use in long-timescales is an open question.

For this reason we will not discuss parameters that describe sediment flux dependence in the context of a GTL. This decision highlights the double-edge of short-timescale studies in constraining GTLs. The dynamics of sediment transport, impacts, and cover can be studied on event and seasonal timescales—this results in observations of complexities that are difficult to implement on long timescales, in models that do not explicitly resolve events (or even discharge), and do not formally represent channel width. We discuss this further in Section 7.5.

5.1.3. Methods to Estimate the Detachment-Limited Erodibility, K

The most common approach to estimate values for the erodibility coefficient is to use well-constrained river systems in which an initial condition topography is known. m , n , and K are then estimated to minimize the misfit between observed and end-of-model-run topographic profiles (Gran et al., 2013; Hobbey et al., 2011; Rosenbloom & Anderson, 1994; Stock & Montgomery, 1999; Valla et al., 2010; van der Beek & Bishop, 2003; Whipple, Snyder, et al., 2000). We omit the results of Tomkin et al. (2003) because they did not find acceptable fits for the detachment-limited model. Comparison of alternative incision models indicates that multiple formulations can make reasonable fits with the same topographic data at a given site (Hobbey et al., 2011; Valla et al., 2010; van der Beek & Bishop, 2003), indicating either that different landscapes require different models, or that comparison techniques struggle to resolve differences between models.

As described above, we focus here on coefficients relating E with A and S . We thus omit from this compilation the results of Lavé and Avouac (2001) because they present a K -like constant in terms of excess nondimensional stress (defined below in equation (22)). We also omit the work of Garcia-Castellanos and O'Connor (2018) who present their estimates in terms of excess shear stress and focus on outburst floods. While such events can be constrained, their hydraulics differ substantially from most river systems. These are two studies that fit the uncommon category of having sufficient constraints to estimate channel hydraulics in the geologic past.

Another approach is to use knickpoint retreat models to estimate values for K (Berlin & Anderson, 2007; Crosby & Whipple, 2006). We only make a tentative comparison with these two studies as knickpoints are areas where flow hydraulics and erosion processes are known to deviate significantly from the assumptions of steady uniform flow that underpin the derivation of the equation containing K .

The final approach for estimating K that we discuss is that of Harel et al. (2016) who compiled 1,457 ^{10}Be catchment-averaged erosion rates from around the world and compared them with topographic indices. Calculated K values range globally by approximately 15 orders of magnitude (from 10^{-15} to 10^0 yr^{-1} , the min-max range of Harel et al. (2016, Figure 6 “global” panel), with median global K being $2.9 \times 10^{-10} \pm 1.0 \times 10^{-9} \text{ yr}^{-1}$. This approach assumes that catchment-averaged erosion rates are representative of river incision and but does not assume that basins are in topographic steady state.

Some of the trends in K values reported by Harel et al. (2016) follow expected patterns. For example, average K values found in rivers eroding igneous rocks are several orders of magnitude lower than those found in rivers eroding sedimentary rocks. While not directly comparable, this result is consistent with that of Garcia-Castellanos and O'Connor (2018) who found a consistent relationship between lithology and erodibility and found variations of 2 orders of magnitude within lithology classes. Additionally, the variability in K within a given climatic or lithologic regime is substantially less than the global range. The results of Harel et al. (2016) support the conclusion that global variability in K is enormous, but that K is less variable within a specific field site.

5.1.4. Unit Conversions and Estimates of K

Identifying appropriate a priori values for the erodibility constant K is difficult given the number of variables wrapped up in these parameters (e.g., Whipple, Hancock, et al., 2000). However, a number of researchers have sought to infer effective values of K from field, topographic, and geochronologic data (Table 3). In many cases authors considered both detachment-limited and transport-limited formulations in fitting observations with theory.

Table 3
Unconverted Erodibility Coefficient, K

Coefficient	Units	Reference	Method
0.11	$m^{0.22}yr^{-1}$	Howard and Kerby (1983)	Least squares regression of measured erosion rate, drainage area, and slope
4.1×10^{-7} to 1.1×10^{-2}	$m^{0.2}yr^{-1}$	Stock and Montgomery (1999)	Comparison of topographic profiles and stream power model
2.4×10^{-4} to 9.0×10^{-4}	$m^{0.2}yr^{-1}$	Whipple, Snyder, et al., (2000)	Natural experiment of incision over ~100 years
7.0×10^{-7}	$m^{0.4}yr^{-1}$	van der Beek and Bishop (2003)	Comparison of topographic profiles and a detachment limited stream power model
10^{-6}	$m^{0.4}yr^{-1}$	van der Beek and Bishop (2003)	Excess stream power model
7.9×10^{-9}	$m^{1-2m}yr^{-1}$	Crosby and Whipple (2006)	Knickpoint retreat model
3.33×10^{-8} to 2.87×10^{-7}	$m^{1-2m}yr^{-1}$	Berlin and Anderson (2007)	Knickpoint celerity model
10^{-15} to 10^0	yr^{-1}	Harel et al. (2016)	Comparison of ^{10}Be catchment-averaged erosion rates and topographic indices

The values of m and n (or m_t and n_t) used in and within each of these studies vary because the scaling exponents are often parameters fit by minimizing model data misfit. However, changing the value of m or m_t changes the units of K . We thus convert the reported values of K into a form with consistent units (Table 4). One of the complications associated with the area slope erosion law is that the units of K depend on the exponent m , estimates of which vary among different studies. It is impossible to meaningfully compare K values with different units. We converted published K values into standardized (and therefore comparable) values with consistent units, using reference values of the exponents m and n .

To convert from a published erosion coefficient value, denoted here as K_p , with slope and area exponents of m_p and n_p , to a standardized value K_c , we need reference values of m and n (denoted as m_r and n_r), a reference slope S_r and a reference area A_r . The standardized erosion coefficient, K_c , is obtained from

$$K_c = K_p A_r^{(m_p - m_r)} S_r^{(n_p - n_r)}, \quad (18)$$

with $m_r = 0.5$, $n_r = 1$, using two reference values of drainage area A_r (10^6 and 10^7 m²) and two reference values of slope S_r (0.1 and 0.01). The values chosen for m_r and n_r reflect the assumption that E goes linearly with stream power. A more extensive discussion of exponent values is presented in section 5.4. The use of two A_r and two S_r values yields four different values of K_c for each K_p estimate; for any given K_p value, the resulting range of K_c may span orders of magnitude.

Clearly, the results of conversion depend on the values of A_r and S_r . Here the reference areas and slopes were chosen to reflect a relatively small, steep catchment. While this approach is heuristic, it allows us to extract estimates of K from studies that find a wide range of best fit m and n values (e.g., van der Beek & Bishop, 2003). Short of recomputing long profile model fits with standardized m and n values, we know of no other way to standardize the units of K , as there is no single characteristic slope and drainage area with which to standardize K . The values calculated in this manner are “comparable” in that they have the same units. It is difficult to assess the extent to which they compare to refitted estimates with consistent m and n without undertaking such an exercise. The issue of comparable K s is further discussed in section 7.3

Note that Table 4 excludes values reported from studies that (a) were focused on modeling knickpoint retreat (Berlin & Anderson, 2007; Crosby & Whipple, 2006), or (b) used equations requiring other variables to be calculated, measured or assumed a priori. Examples of these include transport-limited formulations requiring a median grain size (D_{50}), shear stress-based models including a critical shear stress term, or sediment flux-dependent river incision models (e.g., Hobbey et al., 2011; van der Beek & Bishop, 2003).

Table 4
Selected Converted Simple Stream Power Erodibility Coefficient (K) Values

A (m ²)	S	K (y ⁻¹)	Reference	Lithology
10 ⁶	0.1	1.03 × 10 ⁻⁷ to 2.8 × 10 ⁻³	Stock and Montgomery (1999)	Lithology varies from granite to mudstone
10 ⁷	0.1	8.18 × 10 ⁻⁸ to 2.2 × 10 ⁻³		
10 ⁶	0.01	1.03 × 10 ⁻⁷ to 2.8 × 10 ⁻³		
10 ⁷	0.01	8.18 × 10 ⁻⁸ to 2.2 × 10 ⁻³		
10 ⁶	0.1	0.10	Howard and Kerby (1983)	Clayey sand
10 ⁷	0.1	0.09		
10 ⁶	0.01	0.21		
10 ⁷	0.01	0.18		
10 ⁶	0.1	2.26 × 10 ⁻⁴ to 6.03 × 10 ⁻⁵	Whipple, Snyder, et al., (2000)	Sandstone
10 ⁷	0.1	1.78 × 10 ⁻⁴ to 4.79 × 10 ⁻⁵		
10 ⁶	0.01	2.26 × 10 ⁻⁴ to 6.03 × 10 ⁻⁵		
10 ⁷	0.01	1.78 × 10 ⁻⁴ to 4.79 × 10 ⁻⁵		
10 ⁶	0.1	2.0 × 10 ⁻⁹	van der Beek and Bishop (2003) Detachment Limited m=n=1	Metasedimentary and metavolcanics
10 ⁷	0.1	6.32 × 10 ⁻⁹		
10 ⁶	0.01	2.0 × 10 ⁻⁹		
10 ⁷	0.01	6.32 × 10 ⁻⁹		
10 ⁶	0.1	1.18 × 10 ⁻⁷	van der Beek and Bishop (2003) Detachment Limited m=0.4, n=1	Metasedimentary and metavolcanics
10 ⁷	0.1	9.38 × 10 ⁻⁸		
10 ⁶	0.01	1.18 × 10 ⁻⁷		
10 ⁷	0.01	9.38 × 10 ⁻⁸		

5.2. Representation of Channel Width and Grid-Scale Dependence

The focus of this contribution is in parameter values for GTLs rather than numerical implementation. In this section we make an exception and discuss the representation of channels in numerical implementations of GTLs for water erosion because of a documented grid-scale dependence of 2-D model behavior (e.g., Perron et al., 2008; Schoorl et al., 2000). This dependence occurs because contributing area is grid-scale dependent for planar (but not convergent) regions of topography (Pelletier, 2010) and because valley bottoms are not resolved by the 2-D domain. Models which represent a channel-long profile through a single 1-D profile or a network of profiles do not suffer from this scale dependence. In contrast, 2-D models that use drainage area may suffer from scale dependence because they contain a network of 1-D channels embedded in a 2-D mesh of hillslopes.

When detachment-limited erosion is implemented in a 2-D model some authors propose use of a correction factor or algorithmic adjustment in order to remove a grid cell size dependence (Armitage, 2019; Howard, 1994; Perron et al., 2008; Pepin et al., 2010; Passalacqua et al., 2006; Pelletier, 2010). This grid-scale dependence is potentially problematic for inversion of landscapes using 2-D numerical implementations to infer absolute, scale-independent values for K because the estimated value may be sensitive to the grid cell size. We note that when an inversion approach is used in the studies discussed in the prior section, a 1-D channel profile model was used, and these 1-D-based estimates would not be expected to include any grid-scale bias.

Whether inversions using 2-D numerical implementations to infer K from natural experiments are sensitive to the documented grid-scale dependence or any of the proposed approaches to address it is an open question that is worthy of further investigation. Ultimately the importance of scale effects depends on the

use, interpretation, and intended transferability of an inferred value of K , as well as the relative sources of uncertainty in its estimate.

5.3. Transport-Limited Incision Rate: Forms of q_s and the Parameter K_t

5.3.1. Theoretical Background

In settings where the detachment of material from the ground is not limiting, the rate of change of the elevation of the land surface is described by the divergence of sediment flux (equation (10)). Mathematical statements describing the modification of topography due to gradients in sediment carrying capacity are based on laboratory flume and field measurements of sediment flux, typically bedload. These expressions are often called “transport limited.”

Many sediment transport formulas describe the relationship between the dimensionless Einstein bed load number q^* , the nondimensional boundary shear stress (Shields stress) τ^* , and sometimes the critical Shields stress τ_c^* :

$$q^* = f(\tau^*) \quad (19)$$

or

$$q^* = f(\tau^*, \tau_c^*), \quad (20)$$

with q^* is defined as

$$q^* = \frac{q_s}{D_s \sqrt{R_b g D_s}}. \quad (21)$$

and τ^* given as

$$\tau^* = \frac{\tau}{\rho_w R_b g D_s} \quad (22)$$

where τ is the dimensional boundary shear stress, ρ_w is the density of water, R_b is the nondimensional bouyant density ($R_b = (\rho_s - \rho_w)/\rho_w$), g is gravitational acceleration, and D_s is the grain size. Formulations that consider multiple grain size fractions have been developed (e.g., Wilcock & Crowe, 2003) but we do not consider them here for the sake of brevity.

Many empirical sediment transport equations (e.g., Meyer-Peter & Müller, 1948; Wong & Parker, 2006) can be synthesized to the form

$$q^* \sim (\tau^* - \tau_c^*)^{3/2}, \quad (23)$$

while the Einstein-Brown equation (Einstein, 1950; Howard, 1994; Willgoose et al., 1991a) can be approximated by

$$q^* \sim (\tau^*)^3. \quad (24)$$

Despite the diversity of sediment transport formulae, when employed as a GTL they are commonly simplified to the form

$$q_s = \frac{Q_s}{W} = \frac{K_t A^{m_t} S^{n_t} - \omega_{t,c}}{W} \quad (25)$$

where Q_s is the volumetric sediment flux, W is flow width, K_t is an erodibility coefficient, m_t and n_t are positive dimensionless coefficients, and $\omega_{t,c}$ is a threshold for transport that may or may not be included (e.g., Hancock et al., 2010, 2018; Smith & Bretherton, 1972; Tomkin et al., 2003; van der Beek & Bishop, 2003; Valla et al., 2010). Equation (25) incorporates the basin hydrology and channel hydraulic geometry scaling of equations (16) and (17) as well as a friction relationship to calculate τ . When the threshold for transport is omitted it may be done for analytical reasons or because the authors argue that the threshold is negligible for flows of interest. The following section determines values for K_t , m_t , n_t , and $\omega_{t,c}$ using this approach.

5.3.2. Relating q_s to A and S

To express q_s as a function of A and S , one must start from a sediment transport formula. We present here an example of how to do this, using the Meyer-Peter Müller formula of Wong and Parker (2006). Our derivation is similar to that of Gasparini et al. (2004) and Willgoose (2018, his equation (4.15)). We begin by converting equation (23) to the dimensional form.

$$q_s = \frac{3.97}{\rho_w^{1.5} R_b g} (\tau - \rho_w R_b g D_s \tau_c^*)^{1.5}. \quad (26)$$

For $q^* \sim (\tau^* - \tau_c^*)^{1.5}$ scaling, the grain size, D_s , remains in the threshold portion of the equation representing the dimensionalized form of τ_c^* . If Einstein-Brown scaling $q^* \sim (\tau^*)^3$ is used, then no threshold is present but $q_s \sim (D_s)^{-1.5}$.

Assuming uniform flow in a wide channel, we can write $\tau \approx k_f q^\alpha S^\beta$ with q as surface water discharge per unit width, k_f , α , and β as constants whose values can be derived from a friction law such as the Manning equation or Darcy-Weisbach equation (Tucker, 2004). For the Manning equation $\alpha = 3/5$, $\beta = 7/10$, and $k_f = \rho_w g n_m^{3/5}$, where n_m is the roughness. For the Darcy-Weisbach equation $\alpha = 2/3$, $\beta = 2/3$, and $k_f = (\rho_w g^{2/3} f^{1/3}) / 2$, where f is the roughness parameter. Incorporating this into equation (26), multiplying by W to acknowledge that $Q_s = W q_s$, and simplifying the exponent by distributing it yields

$$Q_s = \frac{3.97W}{\rho_w^{1.5} R_b g} \left[(k_f q^\alpha S^\beta)^{1.5} - (\rho_w R_b g D_s \tau_c^*)^{1.5} \right] \quad (27)$$

Combining our equations for basin hydrology and channel hydraulic geometry (equations (16) and (17)) we can get an expression for q in terms of A

$$q = \frac{k_q^{(1-c_w)}}{k_w} A^{c_q(1-c_w)}. \quad (28)$$

Substituting equation (28) into equation (27) and reorganizing to obtain a form of $Q_s = K_t A^{m_t} S^{n_t}$ we obtain expressions for $m_t = 1.5\alpha c_q^2 c_w (1 - c_w)$, $n_t = 1.5\beta$,

$$K_t = \frac{3.97}{R_b g} \left(\frac{k_f k_q^{\alpha c_w (1-c_w)}}{\rho_w k_w^{(\alpha-2/3)}} \right)^{1.5}. \quad (29)$$

and

$$\omega_{t,c} = 3.97 k_w k_q^{c_w} A^{c_w c_q} (R_b g)^{0.5} (D_s \tau_c^*)^{1.5} \quad (30)$$

The dependence of $\omega_{t,c}$ on drainage area reflects the dependence of shear stress on discharge over width, each of which are represented by a scaling relationship with drainage area (equations (16) and (17)). In the next section, we provide a back-of-the-envelope calculation of K_t .

5.3.3. Estimates of the Transport-Limited Erodibility, K_t

We describe three approaches for determining the value of K_t . One follows directly from empirical sediment transport formulas, the algebra for which was presented in the prior section. The second and third approaches infer effective values for K_t , m_t , and n_t over a study timescale given either (a) observations of runoff, discharge, and sediment loss or (b) channel long profiles.

In the first approach we perform a back-of-the-envelope calculation of K_t using equation (29). We identify plausible ranges input values and use them to identify a bounding range for K_t .

Some of the coefficients required to calculate K_t in this way are readily available. For example, $\rho_w = 1,000 \text{ kg m}^{-3}$, and given a wide range of sediment densities of $\rho_r = 1,200\text{--}3,300 \text{ kg.m}^{-3}$, $R_b = 0.2\text{--}2.3$. While ρ_r for volcanic ash or scoria is less than $1,000 \text{ kg m}^{-3}$, we consider this a fringe case; for quartz grains in water, $R_b \approx 1.65$. For natural channels, Manning's coefficient n_m varies from $0.01\text{--}0.1 \text{ m}^{-1/3}\text{s}$ (Barnes, 1967; Bathurst, 2002), while the Darcy-Weisbach roughness parameter from $0.01\text{--}1$ (unitless) (Bathurst, 2002; Wong & Parker, 2006). These ranges results in comparable ranges for τ .

The scaling exponent between discharge and channel width is commonly assumed to be $c_w \sim 0.5$ (Leopold & Miller, 1956; Wohl & David, 2008). We consider a range of $c_w = 0.37\text{--}0.62$ based on the 95% confidence interval of Wohl and David (2008). Using $c_w = 0.5$, data presented in Leopold and Maddock (1953) implies that $k_w = 5.5\text{--}9.1 \text{ m}^{-0.5} \text{ s}^{0.5}$. The scaling exponent between discharge and area c_q commonly ranges between 0.7 and 1, depending on the choice of representative discharge (such as mean annual versus bankfull) and the basin characteristics (Dunne & Leopold, 1978).

The parameter k_q is more difficult to constrain. Recall that it relates scaled drainage area to discharge, but is applied within a theoretical framework that assumes steady uniform flow. Thus, it must represent the shear stress imparted by a geomorphically effective event—likely constrained to short time periods relative to geomorphic timescales. The implicit assumption in this formulation is that the discharge approximated by $k_q A^{c_q}$ is appropriate to apply uniformly in time. It represents an effective discharge, whose net geomorphic impact is equivalent to that of a natural sequence of flow events of varying frequency and magnitude. In principle, the effective value of k_q can be linked to the statistics of either stream flow or precipitation (Lague et al., 2005; Molnar, 2001; Tucker & Bras, 2000; Tucker, 2004; Willgoose et al., 1991a), though reviewing this connection lies beyond the scope of this contribution. Here we attempt to constrain the order of magnitude of k_q in the case where c_q is unity, and take as bounding values the order of magnitude of rainfall ($0.001\text{--}30 \text{ m.yr}^{-1}$).

The dimensions depend on the values of c_w , c_q , and α . Assuming $c_w = 0.5$, $c_q = 1$, and $\alpha = 2/3$ (Darcy-Weisbach friction relationship) the dimensions would be $[\text{LT}^{-1}]$. Across all permutations (and thus variable units) we obtain a range for K_t of $10^{-4}\text{--}10^{-1} \text{ m.yr}^{-1}$. Variation is primarily controlled by the value of the drainage basin hydrology coefficient k_q .

A second approach is to estimate K_t based on long channel profile fits, similar to that described in Section 5.1.3 and was taken by Tomkin et al. (2003), van der Beek and Bishop (2003), and Valla et al. (2010). Among these, only Valla et al. (2010) found that a transport-limited erosion law successfully accounted for the observed longitudinal profile morphology at their study site. They reported estimates of K_t ranging from 2×10^{-6} to $3 \times 10^{-5} \text{ m.yr}^{-1}$ ($m_t = n_t = 1$).

A third approach determines estimates a value for K_t by relating the observed discharge and sediment flux data. This approach has been used, for example, to estimate channel sediment transport parameters for the SIBERIA numerical model (Hancock et al., 2000; Moliere et al., 2002; Willgoose & Riley, 1998). Several studies have taken this approach (Hancock & Willgoose, 2001; Hancock et al., 2000, 2010, 2011, 2018; Moliere et al., 2002; Willgoose & Riley, 1998, 2002). Data deriving from such studies can in principle be used to estimate effective values of K_t (note that incomplete reporting of units in the above studies precludes including their results in Table 2).

5.4. Discharge and Slope Exponents m , m_t , n , and n_t

For detachment-limited and erosion-deposition models, there are a few permutations of the values of m and n , each derived from a different set of assumptions regarding physical processes. In this way, changing a value of m or n may be considered the construction of a different model.

If one assumes that the rate of river incision depends on stream power per unit surface area and the channel width is proportional to the square root of discharge, then $m = 1/2$ and $n = 1$ (Whipple & Tucker, 1999). Use of total stream power yields $m/n = 1$ (Seidl & Dietrich, 1992; Seidl et al., 1994). If instead of stream power, one uses the shear stress τ , then the values of m and n depend on the formula for channel roughness. Use of the Manning equation yields $m = 3/5$ and $n = 7/10$ (Howard & Kerby, 1983; Howard, 1994), while use of the Darcy-Weisbach roughness law yields $m = 1/3$ and $n = 2/3$ (Tucker & Slingerland, 1997).

Additional considerations in setting m and n may be derived from a known physical mechanism of detachment. Whipple, Hancock, et al. (2000) suggest, on the basis of a theoretical argument, that detachment-limited slope exponent n between $2/3$ and 1 is consistent with erosion by plucking, while an exponent of $\sim 5/3$ is consistent with suspended-load abrasion. Differences in m can reflect different scaling in the relationship between channel width and drainage area (Snyder et al., 2003; Wohl & David, 2008). In principle, for a drainage network undergoing steady, uniform erosion of homogeneous material, the m/n ratio is equal to the concavity index, θ , defined by

$$S = A^{-\theta}, \quad (31)$$

where S is channel gradient and A is drainage area (Whipple & Tucker, 1999). Observed concavities range from < 0.3 to > 1.0 , with most values close to 0.5 (see summary in Tucker & Whipple, 2002).

As with the detachment-limited exponents, the transport rate exponents m_t and n_t combine information about use of unit stream power or shear stress, the hydraulic geometry, and the sediment transport expression that relates q^* with τ^* and τ_c^* . The use of the Manning equation, a wide channel, and the Einstein-Brown formula yields $m_t \sim 2$, $n_t \sim 2$ for sand rivers with active sediment transport (Smith & Bretherton, 1972; Willgoose et al., 1991a). Such values are consistent with observed channel concavities given the transport-limited concavity $\theta_t = (m_t - 1) / n_t$. If instead the simplification relies on one of the many sediment transport relationships that scale as $\sim(\tau^*)^{1.5}$, the value for n_t is 1 for both the shear stress and stream power forms and m_t depends on the scaling of drainage area and channel width with discharge and specifics of the friction law used (Whipple & Tucker, 2002). Wickert and Schildgen (2019) argue for $n_t = 7/6$ and for empirical derivation of m_t .

The values of m and m_t are additionally significant because the units of K and K_t depend on them. For $E = KA^m S^n$, K has dimensions of $[T^{-1} L^{(1-2m)}]$ and for $Q_s = K_t A^{m_t} S^{n_t}$, K_t has dimensions of $[T^{-1} L^{(3-2m_t)}]$. As such we provide a methodology below to convert K to standard units.

5.5. Erosion Thresholds, ω_c and $\omega_{t,c}$

Both expressions for erosion by flowing water have a critical shear stress that must be exceeded in order for incision to occur (equations (13) and (14)). First, consider the expression for detachment-limited incision in equation (9), which includes a threshold ω_c . If erosion rate is assumed to scale with shear stress, then $\omega_c = k_e(\tau_c)^a$, while if stream power is used, the threshold is $\omega_c = k_e(\tau_c U_c^*)^a = k_e(\tau_c \sqrt{\tau_c / \rho_w})^a$. Zero is the lower bound for τ_c and k_e is poorly constrained. a depends on the dominant mechanism of removing material and likely ranges from 1 to 7/2 (Whipple, Hancock, et al., 2000).

An estimate of the critical shear stress for the transport limited case, τ_c , can be found using the Shields equation (equation (22)). In a review of published estimates of critical Shields stress, Buffington and Montgomery (1997) identified a range of $\tau_c^* = 0.03$ – 0.08 . When a D_{50} is known, this can be used to calculate a dimensional value. When used in the context of the transport-limited GTL (equation (10)) the form presented in equation (30) can be used.

There are several potential influences on ω_c that we neglect because they are not commonly implemented in models on geologic timescales. These include dependence of the critical Shields stress on local bed slope (Lamb, Dietrich, & Venditti, 2008; Prancevic et al., 2014), relative roughness (Prancevic & Lamb, 2015), history dependence on the magnitude of prior flows (Masteller et al., 2019), variations between alluviated and bare bedrock stretches (Ferguson et al., 2017), and dependence on the state of q_s (Johnson, 2016).

For detachment-limited erosion, the critical shear stress may be higher than that in the transport-limited case. Tucker et al. (2006) compiled values for bare and grass-covered soils, with a range of critical shear stress values from 0.6 to over 240 Pa. Assuming the density of quartz, this corresponds to a grain size range of 3×10^{-4} to over 3×10^{-1} m. Higher critical shear stress values are likely for unfractured bedrock. However, Lavé and Avouac (2001) found that a value of $\tau_c^* = 0.03$ was consistent with patterns of fluvial incision across the Himalaya.

The variation in estimates for ω_c may reflect the variation in the mechanistic origin of the erosion threshold for detachment-limited erosion. Detachment of material may occur due to plucking, entrainment, or abrasion (Whipple, Hancock, et al., 2000). Sklar and Dietrich (2004) argue that the threshold energy for a bedload impact to detach material is small relative to the threshold to initiate bedload transport. Thus, values of ω_c that reflect common critical Shields stress for transport-limited erosion may indicate an importance of sediment flux-dependent incision.

6. Connecting Changes in the Precipitation Distribution to Changes in K and K_t

The compilation in section 5 clearly documents the evidence that the parameters K and K_t vary across orders of magnitude and that, as written in forms such as equation (9), these parameters include basin hydrologic relationships. The benefit of using drainage area A instead of surface water discharge Q in GTLs for erosion by water (equations (9) and (10)) is that hydrology need not be explicitly represented. However, erosion

by water involves a link between climate and the evolution of Earth's surface. An important question that remains is, how do changes in climate manifest in changes in K and K_r ?

In keeping with our defined Approach and Scope, here we focus on practical efforts to use GTLs at specific location. Our aim is to describe an approach used to address this issue in the context of the case study described in section 2.1 and in (Barnhart et al., 2020b, 2020c). In the following section we define a methodology to estimate the hydrological parameters necessary to evaluate how K changes as a function of changing precipitation distribution and infiltration capacity. While we only present an approach for K , we note that a similar approach could be applied K_r , by using q_s instead of E .

As discussed in section 5.3.3, precipitation is only one component in a lumped parameter like K and K_r . As such our efforts to connect changes in the distribution of precipitation to K and K_r reflect only one part of understanding how K is impacted by climate; nonetheless, it is an important part. We use the stochastic hydrologic model of Rossi et al. (2016), as applied in a mathematical model of long-term fluvial erosion by Barnhart et al. (2019). This stochastic hydrological model ties the commonly available observation of mean daily rainfall with the geomorphically relevant value of surface water discharge.

Erosion by water is given as a function of $f(p)$ the precipitation distribution (described by p_d , the mean daily rainfall and c the precipitation distribution shape factor), the effective daily infiltration rate I_m , and F the fraction of days in which it rains. Recalling that $Q = (p - I_m)A$ we can write

$$E = F \int_{I_m}^{\infty} K_q (p - I_m)^m A^m S^n f(p) dp = K_q Q^m S^n = KA^m S^n \quad (32)$$

where K_q is the discharged-based erodibility coefficient. We note that I_m is timescale dependent, and here is defined specifically with reference to daily precipitation data.

The complementary cumulative distribution function for daily averaged precipitation intensity is described by a stretched exponential (Rossi et al., 2016). The probability that a random variable P will be greater than p is given as

$$\Pr(P > p) = \exp\left(-\left(\frac{p}{\lambda}\right)^c\right) \quad (33)$$

where

$$\lambda = \frac{P_d}{\Gamma(1 + 1/c)} \quad (34)$$

and $\Gamma()$ represents the gamma function. In order to connect changes in precipitation distribution with changes in K we must evaluate the ratio between the value of K under two different precipitation regimes at $t = t_0$ and $t = t_1$ defined by $f_0(p)$ and F_0 and $f_1(p)$ and F_1 .

$$\frac{K_1}{K_0} = \frac{F_0 \int_{I_m}^{\infty} (p - I_m)^m f_0(p) dp}{F_1 \int_{I_m}^{\infty} (p - I_m)^m f_1(p) dp} \quad (35)$$

Our choice of hydrological model was heavily influenced by a need to constrain it with current and future observations for application in the motivating case study. In contrast, Poisson pulse type models (Eagleson, 1978; Tucker & Bras, 2000) require hourly rainfall, whereas the approach proposed by Lague et al. (2005) and DiBiase and Whipple (2011) treats discharge rather than precipitation. Recent work by Deal et al. (2018) links the distribution of daily rainfall with fluvial incision through a more complex hydrologic model. We do not consider this model because we lack the appropriate parameter estimates. Here we consider only spatially uniform precipitation, though we note that prior work has identified that the spatial scale of precipitation averaging can influence model results (Coulthard & Skinner, 2016).

As an example of constraining K_1/K_0 we describe an approach tied directly to widely available data sets, for estimating modern and future values for the mean daily rainfall p_d , the precipitation distribution shape factor c , and the intermittency F . Using equation (35) also requires a value for I_m that is appropriate for a daily timescale and an entire-watershed spatial scale. We end this section by estimating values for K_1/K_0 at the motivating case study site.

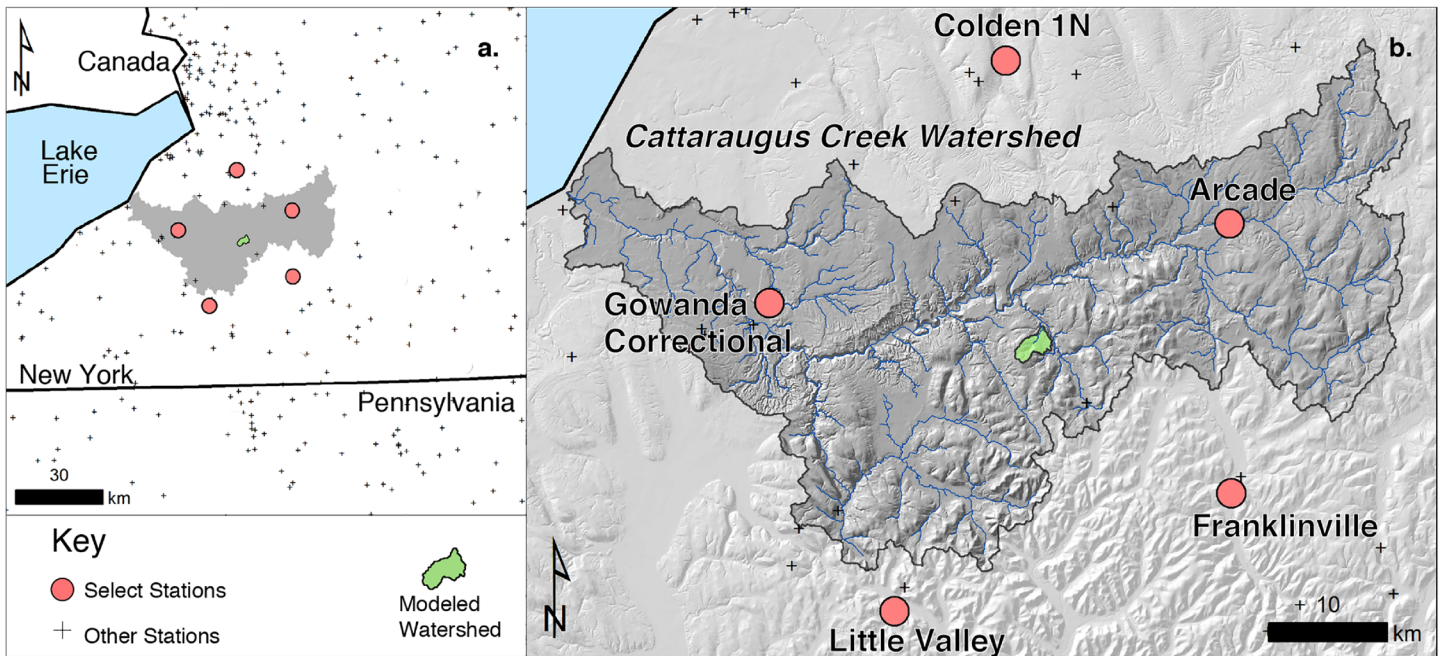


Figure 1. Regional (a) and local (b) maps of GHCN stations used in this analysis. Red symbols show the closest stations to the study site with long, complete records with which to estimate daily precipitation parameters. Yellow symbols show stations used to compare estimates from points to those from daily, gridded precipitation. The Buttermilk Creek catchment is highlighted in green in (b) for reference.

6.1. Precipitation Parameters: p_d , c , F

We describe an approach to estimate modern and future values of p_d , c , and F using empirical analysis of daily precipitation statistics on a subset of meteorological stations selected from the Global Historical Climatology Network (GHCN) v.3.22 (Menne et al., 2012). While the parameters are site-specific, the methodology is portable to other sites.

6.1.1. Current Values

Daily data were downloaded from the National Oceanic and Atmospheric Administration National Climatic Data Center server (<ftp.ncdc.noaa.gov/pub/data/ghcn/daily/>). Within a 30-km radius of the study watershed, there are 29 GHCN stations, six of which record more than 40 years of observations. We used five of these six stations as representative of local hydroclimatic conditions for the study site (one was excluded because it had less than 60% completeness from 1941–2010) (red stations in Figure 1).

Figure 2 illustrates how parametric estimates for mean daily precipitation intensity (p_d), the precipitation shape factor (c), and the fraction of wet days (F) vary in time for the two longest records (>70 years of observations) near the study watershed. The two sites are a similar distance away from the study site (Figure 1b), yet the Franklinville station is 15% drier than the Little Valley station. Below, we provide a more detailed description for how parameters are estimated and how they vary in space and time.

Mean daily precipitation intensity (p_d) is estimated using the average value for all nonzero days over a given time interval. For the reference period of 1941–2010, the spatial average of p_d for the five local stations (red symbols in Figure 1) is $6.50 \text{ mm}\cdot\text{d}^{-1}$ ($2\sigma = 0.61$), where station records are, on average, 79% complete. At two of these stations, records were long enough to calculate time-varying estimates of p_d (top left panel in Figure 2) over 10-yr intervals. There is no trend in p_d (mean value = $6.93 \text{ mm}\cdot\text{d}^{-1}$; $2\sigma = 0.81$) at the wetter site (Little Valley). There is a weak decreasing trend in p_d (mean value = $6.38 \text{ mm}\cdot\text{d}^{-1}$; $2\sigma = 1.01$) at the drier site (Franklinville). The range used by Barnhart et al. (2020b) is $5\text{--}12 \text{ mm}\cdot\text{d}^{-1}$.

While the stretched exponential distribution performs well in describing the full distribution of events, we follow the lead of Wilson and Toumi (2005) and fit the parametric model to only those events larger than the 95th percentile (Rossi et al., 2016). This allows for the distribution to account for apparent heavy-tailed behavior observed in some daily rainfall distributions (Laherrere & Sornette, 1998). To estimate c , we linearize equation (33) by taking the natural log of both sides twice. This yields a log-transformed version

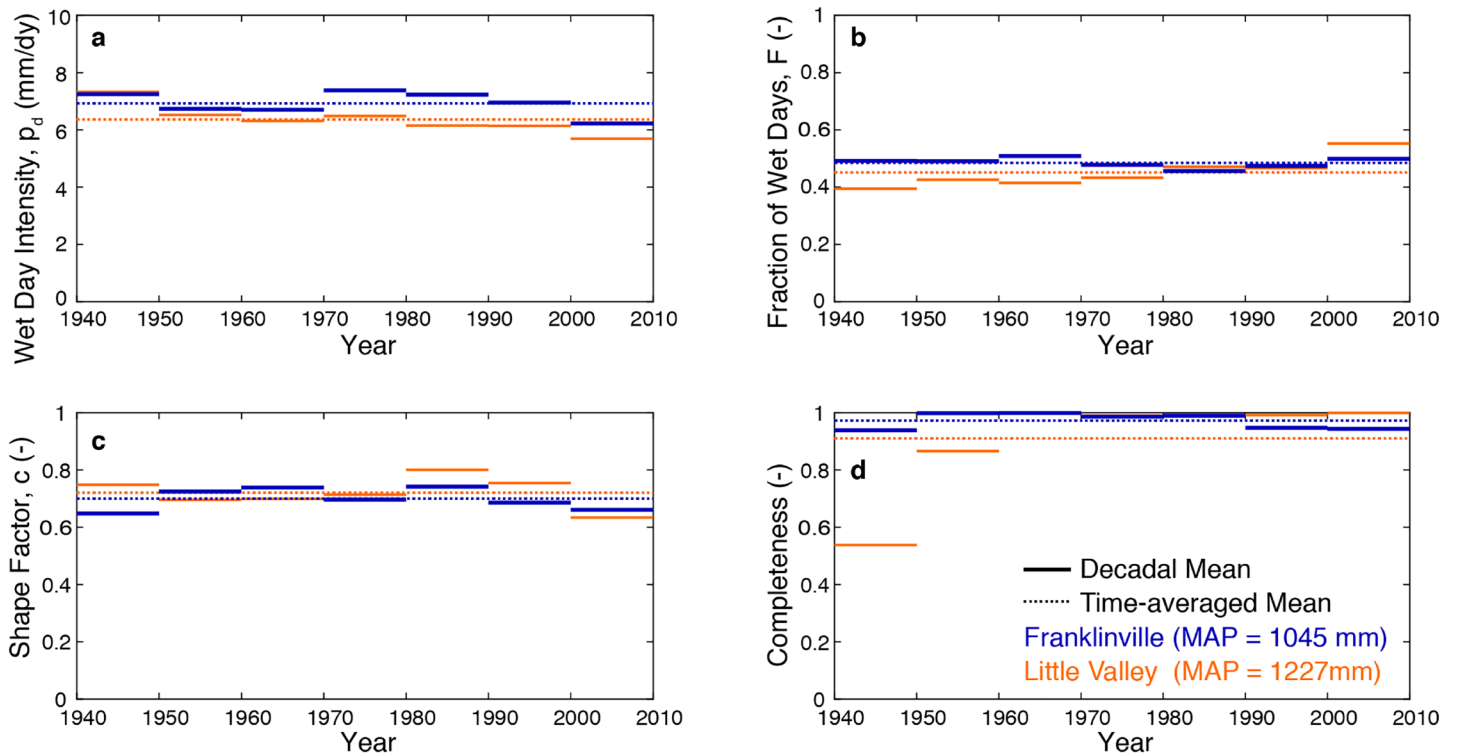


Figure 2. Time-varying estimates (10-year intervals) of daily precipitation parameters from the two local GHCN stations (Figure 1) which have semicontinuous records since the 1940s. Mean daily precipitation intensity (a), fraction of wet days (b), daily precipitation shape factor (c), and the completeness of the record over each interval (d) are shown. Dashed lines show the time-averaged mean value.

of equation (33) that can be evaluated using least squares regression of empirical exceedance frequencies. The slope of the regression line is an estimate of c . Figure 3 shows how well probability distributions are characterized for the five GHCN stations near the study site using this approach.

For the reference period of 1941–2010, the spatial average of c for the five local stations (red symbols in Figure 1) is 0.77 ($2\sigma = 0.03$), where station records are, on average, 79% complete. At two of these stations, records were long enough to calculate time-varying estimates of c (bottom left panel in Figure 2) over 10-yr intervals. There is no trend in c (mean value = 0.70; $2\sigma = 0.07$) at the wetter site (Little Valley). There is also no trend in c (mean value = 0.72; $2\sigma = 0.11$) at the drier site (Franklinville, Figure 2c). This type of regional, multistation analysis can provide not only an estimate of the precipitation distribution's shape factor c , but also an estimate of its uncertainty. The range used by Barnhart et al. (2020b) is 0.6–0.8.

The fraction of wet days (F) is estimated as the ratio of all days with measurable precipitation against all days in the given record. For the reference period of 1941–2010, the spatial average of F for the five local stations (red symbols in Figure 1) is 0.46 ($2\sigma = 0.04$), where station records are, on average, 79% complete. At two of these stations, records were long enough to calculate time-varying estimates of F (top right panel in Figure 2) over 10-yr intervals. There is no trend in F (mean value = 0.49; $2\sigma = 0.04$) at the wetter site (Little Valley). There is a weak increasing trend in F (mean value = 0.45; $2\sigma = 0.11$) at the drier site (Franklinville, Figure 2a). The range used by Barnhart et al. (2020b) is 0.2 to 0.6, which represents the larger value of σ at Franklinville.

6.1.2. Future Values

Next, we describe an approach to estimating how potential future changes in precipitation may be represented using the statistical parameters presented above. As an example, we consider changes over the 21st century; to do so, we build on the latest suite of models coordinated by the Coupled Model Inter-Comparison Project 5 (CMIP5) as best estimates for how climate will change through the 21st century, including changes in precipitation (Taylor et al., 2012). Over 40 different modeling groups contributed to this effort. Given the coarse spatial resolution of the General Circulation Models (GCMs) included in CMIP5, we adopt the down-scaled product of Abatzoglou and Brown (2012) for CMIP5 climate projections at the site of the motivating

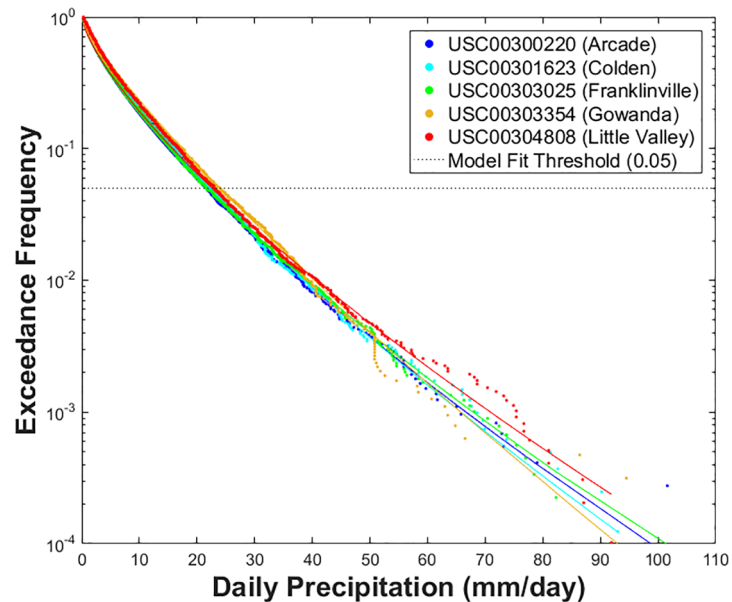


Figure 3. Exceedance frequency plot shows empirical data from five local stations (points) along with the associated best fit, parametric models. Fits are based on least squares regression of ln-transformed data larger than the 95th percentile (dashed line)

case study. Daily precipitation for 20 of the CMIP5 models (one ensemble run only) are included in this downscaled data product. Below, we briefly articulate the rationale for using these data and how they relate to model projections.

Two of the more robust hydroclimatic responses to anthropogenic climate change in global models are an increase in the magnitude of precipitation extremes (O’Gorman & Schneider, 2009; Trenberth, 2011) alongside an increase in dryness, due to lower precipitation frequency and increased evaporative demand (Dai, 2013; Trenberth, 2011). One explanation for these seemingly disparate responses is that, for global increases in temperature, mean annual precipitation increases more slowly than precipitation intensities (Giorgi et al., 2011). This basic system behavior (i.e., increases in both precipitation intensities and in dry spell lengths) is corroborated by the latest CMIP5 experiments (Lau et al., 2013). However, how this global increase in hydroclimatic intensity translates into local or regional water balances is complex. To address this, we use the Multivariate Adapted Constructed Analogs (MACA) daily precipitation data product (Abatzoglou & Brown, 2012).

The MACA method is a statistical downscaling of GCMs that has shown skill in resolving heterogeneous meteorological conditions in the contiguous United States. The success of the method lies in its multivariate approach in downscaling physical variables and its reliance on synoptic-scale (historic) analogs instead of interpolation (Abatzoglou & Brown, 2012). To train the method, a spatiotemporally uniform historic data set is needed. In this study, we used MACAv2-METDATA daily, which was trained on the historic gridded data set METDATA over the years 1979–2012 (Abatzoglou, 2013). Projections on trained models require specification of a Representative Concentration Pathway (RCP) that represents how humans will alter carbon emissions throughout the 21st century. MACA downscaling has been done for two of these pathways (RCP 4.5 and RCP 8.5). Documentation for this downscaling method can be found at <https://climate.northwestknowledge.net/MACA/>. Figure 4 shows the 30-year climate normals derived for 1970–1999 (MACA historic; top panels) and 2070–2099 (MACA RCP 8.5; bottom panels). Mean annual precipitation, mean wet day frequency (>0.8 mm.d⁻¹), and mean wet day intensity (>0.8 mm.d⁻¹) are shown from left to right. While there is substantial spatial heterogeneity in all three precipitation metrics due to topography, coastal proximity, and large-scale circulation patterns, Figure 4 shows two main patterns that have implications for climate futures: (1) mean annual precipitation increases throughout the region over the next century; (2) increases are driven by changes in the mean precipitation intensity, with very little change in the mean wet day frequency.

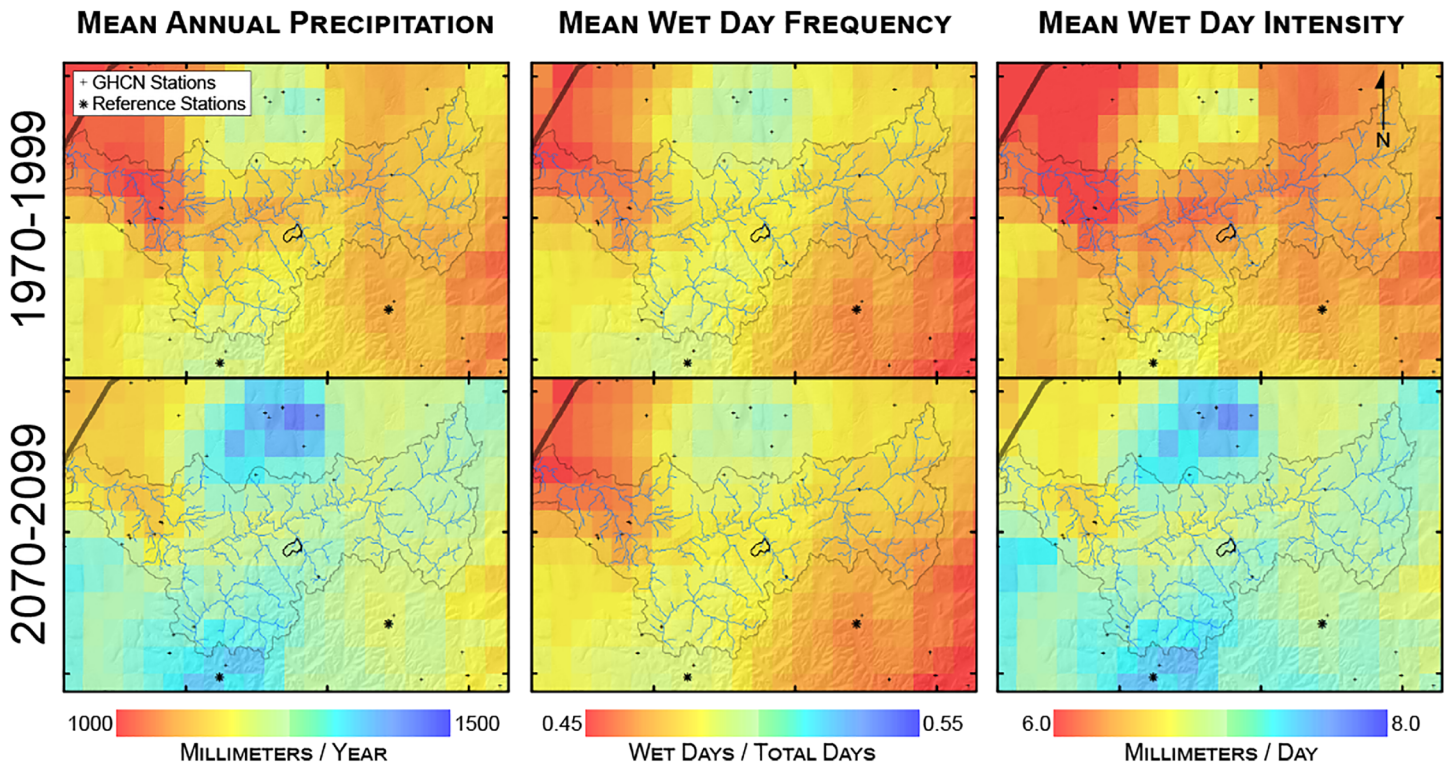


Figure 4. Thirty-year climate normals derived from MACAv2-METDATA daily for mean annual precipitation (left), mean wet day frequency $>0.8 \text{ mm.d}^{-1}$ (center), and mean wet day intensity $>0.8 \text{ mm.d}^{-1}$ (right). Top panels are based on historic training results (1970–1999) and bottom panels are based on RCP 8.5 (2070–2099). Black crosses are locations of all GHCN stations with the two shown in Figure 2 highlighted as large stars. Tick marks on maps are in 15 mile increments and the study watershed is shown using a bold black line.

Figure 5 shows 30-year moving averages (i.e., climatic averages) for mean precipitation, mean wet day intensity ($>0.8 \text{ mm.d}^{-1}$), and mean wet day frequency ($>0.8 \text{ mm.d}^{-1}$) for two emissions scenarios (RCP 4.5 and RCP 8.5). RCP 4.5 emissions peak in the mid-21st century and then decline. RCP 8.5 emissions rise throughout the 21st century and represent the largest magnitude warming considered in CMIP5. Note that values before 2006 are those trained on the historic GRIDMET data set. Figure 5 illustrates in more detail what is driving the 100-year change in climate normals observed in Figure 4, namely, that increases in mean annual precipitation vary in concert with increases in wet day intensity. Furthermore, this time series of climatic

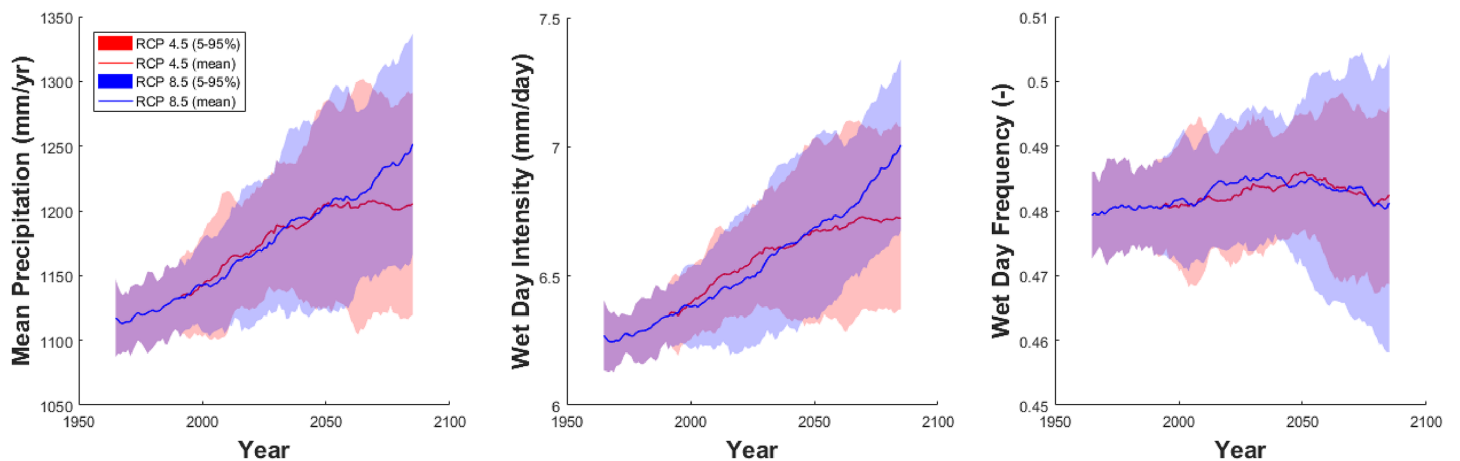


Figure 5. Thirty-year moving averages of mean annual precipitation (left), mean wet day intensity (center), and mean wet day frequency (right) for the MACA grid cell encompassing Frank’s Creek. Ensemble averages ($n = 20$) are shown as solid red (RCP 4.5) and blue lines (RCP 8.5). Shaded areas are 1.64 times the standard deviation of model runs representing the 5th to 95th percentile range.

averages show that increases in wet day intensity (and mean annual precipitation) stabilize midway through the RCP 4.5 scenario and continue to increase throughout the RCP 8.5 scenario.

Based on Figure 5 we identify that at this site changes in precipitation distribution at this site are primarily controlled by an increase of p_d from 6.3 mm.d⁻¹ to a value of 6.7 mm.d⁻¹ for RCP4.5 or 7.0 mm.d⁻¹ for RCP8.5. At other sites, a similar analysis may justify changing values of F and c as well. After discussing soil infiltration capacity, we use the estimated values to calculate K_1/K_0 .

6.2. Soil Infiltration Capacity, I_m

The soil infiltration capacity represents the maximum sustained rate at which rainfall can infiltrate into the soil without generating surface runoff. It is equivalent to the saturated hydraulic conductivity of surface soil, with the caveat that use of daily precipitation means that the infiltration capacity parameter represents an *effective* value: the maximum infiltration rate averaged over a day and over the area of the watershed in question. When possible, ranges for this parameter should be informed by site-specific infiltrometer measurements on representative materials.

An example of how I_m can be estimated comes from the case study (Barnhart et al., 2020b, 2020c). Bennett (2017) conducted 37 infiltration rate measurements at three field locations within the site area. Infiltration rates ranged widely, from 0.5 ± 0.9 mm.hr⁻¹ on the finest-grained, most consolidated sediment, to 852.7 ± 59.6 mm.hr⁻¹ on the coarsest-grained, least consolidated material. The ensemble average among all measured infiltration rates was 32.8 ± 59.1 mm.hr⁻¹. The range measured at the site is broadly consistent with measured infiltration rates for glacial till in other locations, with reported ranges spanning ~ 0.004 to ~ 200 mm.hr⁻¹ (~ 0.4 mm.hr⁻¹ from Strobel, 1993; ~ 0.04 – 40 mm.hr⁻¹ from Mohanty et al. 1994; and ~ 2 – 200 mm.hr⁻¹ from Ronayne et al. 2012).

In order to assess how changes in the precipitation distribution result in changes in K it is necessary to define an infiltration capacity I_m that represents a daily precipitation threshold for runoff generation at the watershed scale. In general, it is expected to be smaller than point-based instrumental measurements described in the prior paragraph. We constrain I_c using mean annual storm runoff, R , in the region (0.2–0.6 m.yr⁻¹, with most estimates closer to the lower end; DOE & NYSERDA, 2010, Appendix F).

The mean annual storm runoff R is related to the precipitation distribution and the infiltration rate:

$$R = F \int_{I_m}^{\infty} (p - I_c) f(p) dp \quad (36)$$

To find the value for I_m consistent with the estimated actual value of $R = 0.2$ m.yr⁻¹, we performed numerical integration of equation (36). Using the precipitation parameters for the reference period of 1941–2010 ($p_d = 6.5$ mm.d⁻¹, $F = 0.46$, and $c = 0.77$), we calculated the corresponding values of R for a range of I_m from 0 to 20 mm.d⁻¹. The value of I_m that best matches $R = 0.2$ m.yr⁻¹ is 15 mm.d⁻¹ (0.625 mm.hr⁻¹ or ~ 5.5 m.yr⁻¹). This falls within the range of the instantaneous, at-a-point measurements reported by Bennett (2017); it is close to the low end of that range, as expected for an effective value that applies to watershed-scale, 24-hr precipitation.

6.3. Estimates of Changes to K

We calculate K_1/K_0 using numerical integration for both the RCP4.5 and RCP8.5 scenarios. For the RCP4.5 scenario, in which F is constant at 0.48, c is constant at 0.82, I_m is constant at 5.5 m.yr⁻¹, and p_d increases from 6.3 to 6.7 mm.d⁻¹ over 100 years (6% increase), K_1/K_0 at the end of 100 years is 1.14. For the RCP8.5 scenario in which all values are the same as the RCP4.5 scenario except that p_d increases from 6.3 to 7.0 mm.d⁻¹ over 100 years (11% increase), K_1/K_0 at the end of 100 years is 1.25. This analysis demonstrates the relationship between changing mean precipitation and K .

7. Discussion

This review highlights challenges in constraining parameter ranges for landscape evolution models and opportunities for future research. We reflect on these challenges before ending with a discussion of processes that lack mature GTLs.

7.1. Variability in Field and Experimental Evidence for Parameter Ranges

Across the reviewed parameters, there is considerable variability in the extent of evidence and theoretical basis for constraining parameter values. The hillslope diffusivity D presents an example of a parameter that is reasonably well constrained using readily available observations of topography (e.g., Richardson et al., 2019). Although the theoretical basis for the parameter itself remains an area of active research (e.g., Anderson et al., 2013; Furbish et al., 2009), there are a number of established methods for estimating its effective value (see discussion in Richardson et al., 2019). The critical Shields stress is an example of a parameter that has both a strong physical basis and a long history of empirical measurement (at least for noncohesive sediment), and one can derive from it an effective threshold for detachment or transport of sediment in fluvial channels.

Reasonably well-constrained parameters can be contrasted with ones such as K and K_t which are challenging to estimate and have bounds that range over orders of magnitude despite decades of study (Harel et al., 2016). One characteristic that makes these parameters challenging is their role as catch-all coefficients that lump together information about erosion mechanisms, climate state, basin hydrology, channel hydraulics, and lithology. It may be tempting to unpack each of these components, as is done for K_t in equation (29). This provides insight into sources of variability in the parameter. On the other hand, the “lumped” form may be the only thing possible to infer from long-term observations of river incision.

The coefficient k_q and scaling exponent c_q which relate discharge and drainage area (equation (16)) provide a good example of a component of K_t that highlights the challenge of connecting what is observable with what is implied by the theoretical derivation—the link between drainage area and geomorphically effective flood assuming steady uniform flow. Estimates for k_q and c_w vary depending on the summary statistic of the discharge distribution used (Sólyom & Tucker, 2004), and the geomorphically effective flood does not occur constantly. These examples highlight a continued need for further research connecting readily observable quantities with parameters suitable for geomorphic timescales.

7.2. The Observation-Application Timescale Mismatch

Another challenge is the mismatch between typical observational timescales and the geologic time frames on which many landscape evolution models are applied. The reviewed parameters include two examples. The at-a-point infiltration rate I_m is straightforward to estimate with field infiltrometer measurements (e.g., Blöschl & Sivapalan, 1995; Gupta et al., 1986; Gentine et al., 2012; Russo & Bresler, 1981). Yet because of the nonlinearity inherent in the process of runoff generation, the instantaneous, point-scale infiltration rate most often is a poor guide when it comes to estimating the effective value I_m —in other words the effective reduction in runoff and erosion due to infiltration and other losses. Instead, measurements that integrate runoff through time and across the scale of a drainage basin may serve as a better time-averaged constraint on this parameter (e.g., Blöschl & Sivapalan, 1995; Gentine et al., 2012; Klemes, 1983; McDonnell et al., 2007; Sivapalan, 2003). For example, an effective I_m could be estimated on the basis of the difference between observed precipitation and event discharge, using baseflow separation to distinguish between event flow and baseflow.

Our example of comparing soil infiltration capacity based on point-based instantaneous measurements and inferring a value from a simple basin-scale hydrologic model illustrate this mismatch. Point measurements ranged from nearly no infiltration to close to a meter per hour with a mean of ~ 30 mm.hr⁻¹ while the basin-scale estimate was half that at about ~ 15 mm.hr⁻¹.

The relationship between the transport limited erosion coefficient K_t and transport formula for sediment flux per unit width q_s also suffers from a potential mismatch in timescale. Empirical estimates for bed load, suspended load, and total load are typically derived from human timescales. Efforts to estimate the parameter most similar to K_t used in the SIBERIA model (called β_1 in Willgoose et al., 1991a, 1991b) at the Ranger Uranium Mine use event-scale discharge and sediment flux observation (Hancock et al., 2000; Moliere et al., 2002; Willgoose & Riley, 1998). Yet instantaneous flume, or event-scale values for K_t may differ from the long term “effective values” due to factors such as nonlinear averaging.

Estimates of geomorphic rates based on cosmogenic nuclide dating typically represent timescales of thousands to hundreds of thousands of years, depending on the application—much longer than the timescale of direct human observation. A potential approach to refine estimates for K_t based on observations on geologic timescales might be combining existing constraints from cosmogenic radionuclides for basin averaged denudation rates (Portenga & Bierman, 2011; Willenbring et al., 2013) with observations of discharge

and contributing area characteristics. This approach would be similar to that done by Harel et al. (2016) but would assume a transport-limited framework and integrate existing discharge observations. Such an approach would not be without limitations. For example, cosmogenic radionuclide samples may be biased due to grain size (e.g., van Dongen et al., 2019) or whether the channel is in an aggradation or degradational phase (e.g., Tofelde et al., 2019).

7.3. The Challenge of Comparable Units

Our review of values for K and K_t in sections 5.1.4 and 5.3.3 highlights a major challenge in synthesizing reported values: when a value for m is estimated jointly with a value for K (or m_t with K_t), values for the erodibility coefficient take on different units and the values become incomparable. Our proposed method accomplishes the goal of converting parameter estimates for K and K_t into equivalent units, but has the unpleasant side effect of increasing the range of estimated values by orders of magnitude. The increase in range derives from using multiple reference slopes and drainage areas in the conversion. While this increase in range is not ideal, the lack of a characteristic slope and drainage area necessitates such an approach. A recommended approach to address the issue of incomparable K values is for authors who estimate K or K_t to fit the parameter both with m or m_t as a free parameter, and with a few standard reference values (e.g., $m = 1/2, 1/3$). This would permit estimation of erodibilities with comparable units as well as the “best fit” erodibility with a free, or otherwise determined exponent. The challenges in inconsistent units in K and K_t come from using the exponents m or m_t as fitting parameters rather than as representative of a fundamental physical relationship. Theoretical justifications can be made for some sets of exponents on the basis of erosion mechanism, though the drainage area exponent—which controls the units of K and K_t —also incorporates the basin hydrology. Further, when the effect of the critical Shields stress is functionally represented as a larger (and thus more nonlinear) exponent, we must ask, “what do these exponents even mean?”

A potential approach to address units that vary based on m and m_t might be the construction of a nondimensional version of A , yet this approach is immediately suspect. First, what characteristic length or area scale is appropriate for a quantity with fractal-like qualities (e.g., Rodríguez-Iturbe & Rinaldo, 2001)? And second, is it even appropriate to expect an exponent that includes basin hydrology to be distilled to a constant that represents a fundamental physical relationship? We might expect a fundamental relationship to emerge from the component of m or m_t that represents the physical process by which shear stress is translated to sediment flux—but this is only one part of the scaling exponent. Addressing these questions is beyond the scope of this contribution. Our intention is to articulate the scope and origin of the challenge of incomparable K and K_t , and highlight the need for a dimensionally consistent approach to estimating effective erosion and transport coefficients.

7.4. Parameter Estimates, Model Assumptions, and Model-Data Fit

In undertaking this compilation we ran into a common problem in which a published effort to constrain a parameter either used a model with assumptions that limit its applicability or in which a model-data fit was poor. We begin by highlighting a few examples.

First, consider the contribution of Petit et al. (2009), which focused on understanding faceted normal-fault-bounded mountain fronts. The study constrained a value for the effective hillslope diffusivity D for steep ($>20^\circ$) facet slopes, through forward model inversion using topographic data for the Weber segment of the Wasatch Fault System, Utah, USA. The value reported for D was $0.13 \text{ m}^2\text{yr}^{-1}$, 4 times higher than the highest value compiled by Richardson et al. (2019) ($D = 0.04 \text{ m}^2\text{yr}^{-1}$ from Riggins et al., 2011). Petit et al. (2009) considered their model fit to be good (best fitting root-mean-square values of around 175 m on a fault facet profile with over 500 m of relief). However, both experimental and field evidence indicate that soil transport on slopes steeper than about 20° will tend to be more rapid than predicted by linear creep theory, motivating the use of a nonlinear diffusion model (e.g., Andrews & Bucknam, 1987, 1999; Roering et al., 1999, 2001). One might argue therefore that the unusually high calibrated D reflects the steepness of the particular terrain in question, and in effect compensates for the lack of a nonlinear term in the equation for soil creep. An estimate obtained in this manner might be considered applicable only to similarly steep slopes.

This example points to the value of multimodel comparison. For example, in comparing multiple, alternative river incision formulae van der Beek and Bishop (2003) were able to identify some formulations that fit the

data better than the others. If one were to reanalyze the site considered by Petit et al. (2009) with both a linear and nonlinear model, it would be possible to discover which model provides a better fit (e.g., Roering, 2008).

In performing multimodel analysis, one is forced to confront the tradeoff between realism and analytical complexity: parameter estimation within more complex models may be more difficult (e.g., Kirchner, 2006; Pfister & Kirchner, 2017). In addition, all else equal, one would expect a model with more parameters to perform better than one with fewer parameters, simply because of the greater degree of freedom to fit data; one can compensate for this by including the number of parameters as a penalty factor in model performance scores, as is done in several commonly used model intercomparison metrics (e.g., AIC or others described by Burnham & Anderson, 2003). One is also forced to confront data limitations, because the ability to constrain certain parameters usually depends on the nature of the data available. The need for a formal statement of performance emphasizes the purpose for which a model was developed (e.g., dynamics, specific outputs). Defining a quantitative performance metric also permits the formal comparison of models with calibrated parameters and those for which no calibration is necessary (Hill & Tiedeman, 2007; Wilcock & Iverson, 2003).

The final example is the work of Harel et al. (2016) to estimate K using a global compilation of cosmogenic radionuclide-based estimates of basin-averaged erosion rate. Implicit in their approach is the assumption that basin-averaged erosion rates, which presumably reflect both gravitational hillslope processes and water erosion processes, can be represented by the stream power expression. One might argue for application of multimodel comparison in this context—yet this may not be feasible on the global scale. Further, it is in undertaking such a global study that Harel et al. (2016) are able to synthesize observations at many sites to come to conclusions that n is generally greater than 1, suggesting that a formal representation of an erosion threshold—which would be expected to produce a similar nonlinear relationship between erosion rate and slope gradient, and has a direct physical basis—may hold merit.

There is value in applying a deliberately simplified model, especially in the context of comparing alternative calibrated models and in interpreting where a model fails. In such an exercise, the parameters of the simpler models are likely to lump together multiple effects (such as the combination of process-related and material-related factors that make up lumped parameters like K and D). The calibrated values of lumped parameters like these may be hard to interpret: the calibration indicates what values minimize model-data misfit, but does not necessarily lend insight into why. This leads to the question: when is a parameter estimate interpretable?

In answering this question we begin by noting that the general character of Earth surface dynamics lends itself to “whataboutisms” of system representation: what about hydrology? what about lithology? what about fracture spacing? what about vegetation? It seems reasonable to expect that all of these effects, and many others, can and do contribute in some fashion to shaping landscapes. But if one’s goal is to understand the essence of a geomorphic phenomenon, then the question inevitably arises: which elements are fundamental, and which only contribute to higher-order details? The answer, of course, depends on the target of study, the nature of data available to test model performance, and the details of how models and data are compared.

The determination that a model for a system or phenomena is sufficient for a specific purpose is inherently subjective. One can never rule out the possibility of achieving better accuracy in explaining or predicting a phenomenon by adding additional layers of theoretical complexity. As a practical matter, the level of complexity in a model should match the theoretical understanding of a phenomenon, the available observational data, and the constraints of the specific problem or question the model is being used to address. Similarly, in interpreting parameter values, one should consider how the estimation was made, whether the estimation is sensitive to the details of the objective function, and under what circumstances the uncertainty in the parameter estimate translates into uncertainty in predicting or understanding the dynamics of a system.

7.5. Difficulties in Establishing Mature and Mechanistic GTLs

In this section, we are motivated by the contrast between sediment flux dependent incision and simple stream power incision. Despite its limitations, simple stream power incision theory is widely used. It can clearly be categorized as a mature and usable GTL. However, the basis for it is broadly empirical. In contrast, as described in section 5.1.2, our mechanistic understanding of sediment flux-dependent incision is much more extensive, supported by event and seasonal-scale field observations and laboratory study.

In its definition based on drainage area, simple stream power incision implies a level of averaging that makes it difficult to investigate at a mechanistic level. Further, theoretical modeling studies have demonstrated that multiple alternative complex formulations can collapse into the form of a simple stream power (Gasparini & Brandon, 2011). In contrast, our collective ability to study the details of sediment flux-dependent incision results in an increasingly complex understanding that makes it more difficult to capture in a formula usable by models which may not resolve individual events or additional state variables such as channel width.

The extensive support for the mechanisms underlying sediment flux-dependent incision only underscores the importance of establishing mature GTLs for this process. We highlight two examples that show possible ways forward. First, Hobbey et al. (2011) perform a forward model inversion exercise that estimates the parameters of a very generic form of $f(q_s/q_c)$. There are some caveats to this approach—for example, it made many simplifications that are known to impact sediment flux dependent incision, such as channel width adjustment and within-event discharge variability. However, for long-term average rates, an “effective” form of $f(q_s/q_c)$ is needed. Further studies constraining such a form in well-constrained natural experiments and connecting general forms to short-term field and laboratory efforts are needed. Second, the approach of Deal et al. (2018) to integrate the joint expression of stochastic precipitation and stream power incision is potentially very powerful to bridge between event and subevent scale phenomena and multiple morphology forming event timescales.

We find an analogy to the ideal gas law useful. This expression describing the relationship between pressure, volume, amount of substance, and temperature of a gas was originally derived empirically based on the synthesis of existing empirical expressions by Clapeyron (1834). It was subsequently connected to statistical mechanics and kinetic theory of gasses. While the groundwork for these disciplines lies in Bernoulli's 1738 *Hydrodynamica*, critical developments that led to the connection between the theoretical and empirical occurred between the 1850s and 1910s through the work of Maxwell, Boltzman, Gibbs, and Einstein.

The stream power incision expression described in equation (9) and efforts to expression generic forms of $f(q_s/q_c)$ are early steps toward our equivalent of an ideal gas law. Work remains to establish more robust equations of state, understand the processes at a mechanistic level, and draw connections between these two lines of inquiry that are appropriate to apply on long timescales. Finally, we note that a key to the success of the ideal gas law is the scale break between individual particle and bulk behavior. It is not obvious whether the processes that move sediment around on the surface of the Earth benefit from such a scale break.

8. Conclusions

The choice of parameter input values is an essential element using geomorphic transport laws, with implications for both the magnitude and trend of model behavior. Motivated by a multimodel application of landscape evolution modeling, we have compiled reasonable ranges for several parameters commonly used in this type of modeling and identified major challenges in linking parameters with observable quantities and theoretical work.

Parameters like the hillslope diffusivity D , the soil production rate P_0 , and the fluvial erosion efficiency K can be based on an extensive literature. K and K_t vary by many orders of magnitude globally. Standard methods for estimating these two parameters result in different units, which we have converted for comparison. This conversion is imperfect due to the absence of a characteristic reference area and slope. Exploring the many approaches to estimating K and K_t highlights the challenge of estimating parameters derived under the assumption of a “geomorphically effective” process using human-timescale observations. We presented an approach that links existing observations and climate model results to constrain precipitation and basin hydrology parameters to understand how changes in precipitation distribution change erodibility coefficients.

Our compilation of parameter estimates for mature GTLs in temperate hillslope and valley terrain underscores the extent of processes that lack such expressions. This includes shallow and deep-seated landsliding, debris flows, nonlocal sediment transport, more complex pedogenic processes, lateral erosion and width adjustment of rivers, and a mature form for sediment flux-dependent incision.

This synthesis serves two purposes. First, it provides a reference and starting point for future studies that apply GTLs and need a starting point for choosing their parameter values. Second, we reflect on common

remaining challenges in parameter estimation. These results motivate a dual effort in (a) developing theory with parameters that can be linked with modern observations, and (b) constraining or unpacking existing parameters.

Code and Data Availability

The creation and analysis of models presented in this three-part series was fully scripted. Instructions for reproducing the results (which took nearly 1 million core hours to run), input files, model and analysis code, and the model output files are available through a GlobusConnect endpoint (endpoint name: Barnhart_WVDP_EWG_STUDY3, endpoint identifier UUID 89df0600-bd11-11e8-8c12-0a1d4c5c824a). In addition, the input files and code are housed on GitHub (https://github.com/kbarnhart/inverting_topography_postglacial) and archived with Zenodo (Barnhart et al., 2020a).

Notation

Names, and, where possible, dimensions for symbols used in the text (length [L], time [T], and mass [M]). Many coefficients have units that depend on dimensionless exponents.

a	Excess shear stress or stream power exponent [-]
c	Precipitation distribution shape factor [-]
c_q	Discharge-drainage area scaling exponent [-]
c_w	Discharge-channel width scaling exponent [-]
f	Darcy-Weisbach roughness parameter [-]
g	Gravitational constant [L T ⁻²]
k_{e1}	Generic erodibility coefficient variable [$M^{-a} L^{a+1} T^{2a-1}$]
k_{e2}	Generic erodibility coefficient variable [$M^{-a} L T^{1-3}$]
k_f	Friction factor. For Darcy-Weisbach formula dimensions are [$M L^{-7/3} T^{-4/3}$]. For Manning dimensions are [$M L^{-11/5} T^{-7/5}$]
k_q	Discharge-drainage area coefficient [$L^{1-3c_q} T^{-1}$]
k_w	Discharge-channel width coefficient [$L^{3-2c_w} T^{c_w}$]
m	Detachment-limited discharge or drainage area exponent [-]
m_p	Published estimate for m or m_t [-]
m_r	A reference value for m or m_t [-]
m_t	Transport-limited discharge or drainage area exponent [-]
n	Detachment-limited slope exponent [-]
n_p	Published estimate for n or n_t [-]
n_r	A reference value for n or n_t [-]
n_t	Transport-limited slope exponent [-]
n_m	Manning's n coefficient [$L^{-1/3} T$]
p	Precipitation rate [LT^{-1}]
q	surface water discharge per unit channel width [L^2T^{-1}]
q^*	Nondimensional sediment flux per unit channel width [L^2T^{-1}]
q_c	Volumetric sediment carrying capacity per unit channel width [L^2T^{-1}]
q_h	Hillslope sediment flux per unit width [L^2T^{-1}]
q_s	Fluvial sediment flux per unit channel width [L^2T^{-1}]
A	Drainage area [L^2]
A_r	Reference drainage area [L^2]
$B_c(x, y, t)$	Boundary condition [LT^{-1}]
E	Modification of the topography by surface water processes [LT^{-1}]
H	Soil/mobile regolith depth [L]
D	Soil creep coefficient [L^2T^{-1}]
D_{50}	Median grain size [L]
D_s	Generic grain size [L]
F	Intermittency, or fraction of days in which it rains [-]
F_0	Value for F for time $t = t_0$ [-]
F_1	Value for F for time $t = t_1$ [-]

H_s	Soil production depth scale [L]
I_m	Infiltration rate
K	Detachment limited stream power erosion coefficient [$T^{-1} L^{(1-2m)}$]
K_0	Value for K at time $t = t_0$ [$T^{-1} L^{(1-2m)}$]
K_1	Value for K at time $t = t_1$ [$T^{-1} L^{(1-2m)}$]
K_c	A converted value of K [$T^{-1} L^{(1-2m_p)}$]
K_p	A published estimate of K [$T^{-1} L^{(1-2m_c)}$]
K_q	Erodibility coefficient using Q instead of A [$T^{-1+m} L^{(1-3m)}$]
K_t	Transport limited stream power erosion coefficient [$T^{-1} L^{(1-3m_t)}$]
P	Precipitation rate random variable [LT^{-1}]
P_s	Soil production rate [LT^{-1}]
P_0	Maximum soil production rate [LT^{-1}]
Q	Surface water discharge [L^3T^{-1}]
Q_s	Volumetric sediment flux [L^3T^{-1}]
R	Mean annual runoff [LT^{-1}]
R_b	Nondimensional buoyant density [-]
S	Slope, defined as positive downward [-]
S_c	Critical slope [-]
U	Water velocity [LT^{-1}]
U_c^*	Critical shear velocity [LT^{-1}]
W	Channel width [L]
α	Exponent on q for calculation of τ [-]
β	Exponent on S for calculation of τ [-]
η	Topographic elevation [L]
η_b	Bedrock elevation [L]
λ	Precipitation distribution scale parameter [-]
ρ_r	Density of bedrock [$M L^{-3}$]
ρ_s	Density of soil/regolith [$M L^{-3}$]
ρ_w	density of water [$M L^{-3}$]
τ	Dimensional shear stress [$M T^{-2} L^{-1}$]
τ^*	Nondimensional shear stress (Shields stress) [-]
τ_c	Dimensional critical stress [$M T^{-2} L^{-1}$]
τ_c^*	Nondimensional critical stress (critical Shields stress) [-]
θ	Concavity index [-]
ω_c	Detachment erosion threshold [LT^{-1}]
$\omega_{c,t}$	Transport erosion threshold [LT^{-1}]
$\Gamma()$	Gamma function [-]

Acknowledgments

Support for this work was provided by a contract with Enviro Compliance Solutions, Inc. (Contract DE-EM0002446/0920/13/DE-DT0005364/001), NSF Award 1450409 to Tucker, an NSF EAR Postdoctoral Fellowship to Barnhart (NSF1725774), and a National Defense Science and Engineering Graduate Fellowship and a University of Colorado Chancellor's Fellowship to Shobe. Landlab is supported by NSF ACI-1450409 and by the Community Surface Dynamics Modeling System (CSDMS; NSF1226297 and 1831623). This work utilized the RMACC Summit supercomputer, which is supported by the National Science Foundation (Awards ACI-1532235 and ACI-1532236), the University of Colorado Boulder, and Colorado State University. The Summit supercomputer is a joint effort of the University of Colorado Boulder and Colorado State University. We acknowledge computing time on the CU-CSDMS High-Performance Computing Cluster. Data storage was supported by the University of Colorado Boulder "PetaLibrary." We gratefully acknowledge Editor Amy East, Associate Editor Jon Pelletier, Tom Coulthard, and two anonymous reviewers for each considering all three manuscripts in the first round of review. In addition, we gratefully acknowledge Editor East, Associate Editor Pelletier, Jens Turowski and one anonymous reviewer for considering the revised version of this manuscript. The constructive and thoughtful comments of all reviewers have substantially improved the manuscripts.

References

- Abatzoglou, J. T. (2013). Development of gridded surface meteorological data for ecological applications and modelling. *International Journal of Climatology*, 33(1), 121–131. <https://doi.org/10.1002/joc.3413>
- Abatzoglou, J. T., & Brown, T. J. (2012). A comparison of statistical downscaling methods suited for wildfire applications. *International Journal of Climatology*, 32(5), 772–780. <https://doi.org/10.1002/joc.2312>
- Anderson, R. S. (2002). Modeling the tor-dotted crests, bedrock edges, and parabolic profiles of high alpine surfaces of the Wind River Range, Wyoming. *Geomorphology*, 46(1-2), 35–58. [https://doi.org/10.1016/S0169-555X\(02\)00053-3](https://doi.org/10.1016/S0169-555X(02)00053-3)
- Anderson, R. S., Anderson, S. P., & Tucker, G. E. (2013). Rock damage and regolith transport by frost: An example of climate modulation of the geomorphology of the critical zone. *Earth Surface Processes and Landforms*, 38(3), 299–316. <https://doi.org/10.1002/esp.3330>
- Andrews, D. J., & Bucknam, R. C. (1987). Fitting degradation of shoreline scarps by a nonlinear diffusion model. *Journal of Geophysical Research*, 92(B12), 12,857–12,867. <https://doi.org/10.1029/JB092iB12p12857>
- Andrews, D. J., & Hanks, T. C. (1985). Scarp degraded by linear diffusion: Inverse solution for age. *Journal of Geophysical Research*, 90(B12), 10,193–10,208. <https://doi.org/10.1029/JB090iB12p10193>
- Armitage, J. J. (2019). Short communication: Flow as distributed lines within the landscape. *Earth Surface Dynamics*, 7(1), 67–75. <https://doi.org/10.5194/esurf-7-67-2019>
- Armstrong, A. C. (1976). A three dimensional simulation of slope forms. *Zeitschrift für Geomorphologie*, 25, 20–28.
- Attal, M., Cowie, P., Whittaker, A., Hobley, D., Tucker, G. E., & Roberts, G. (2011). Testing fluvial erosion models using the transient response of bedrock rivers to tectonic forcing in the Apennines, Italy. *Journal of Geophysical Research*, 116, F02005. <https://doi.org/10.1029/2010JF001875>
- Attal, M., Tucker, G. E., Whittaker, A. C., Cowie, P. A., & Roberts, G. P. (2008). Modeling fluvial incision and transient landscape evolution: Influence of dynamic channel adjustment. *Journal of Geophysical Research*, 113, F03013. <https://doi.org/10.1029/2007JF000893>

- Auel, C., Albayrak, I., Sumi, T., & Boes, R. M. (2017). Sediment transport in high-speed flows over a fixed bed: 2. Particle impacts and abrasion prediction. *Earth Surface Processes and Landforms*, 42(9), 1384–1396. <https://doi.org/10.1002/esp.4132>
- Barnes, H. H. (1967). Roughness characteristics of natural channels. US Geological Survey Water-Supply Paper 1849. <https://doi.org/10.3133/wsp1849>
- Barnhart, K. R., Glade, R. C., Shobe, C. M., & Tucker, G. E. (2019). Terrainbento 1.0: A Python package for multi-model analysis in long-term drainage basin evolution. *Geoscientific Model Development*, 12(4), 1267–1297. <https://doi.org/10.5194/gmd-12-1267-2019>
- Barnhart, K. R., Tucker, G. E., Doty, S., Shobe, C. M., Glade, R. C., Rossi, M. W., & Hill, M. C. (2020a). Calculation package: Inverting topography for landscape evolution model process representation. Zenodo. <https://doi.org/10.5281/zenodo.2799489>
- Barnhart, K. R., Tucker, G. E., Doty, S., Shobe, C. M., Glade, R. C., Rossi, M. W., & Hill, M. C. (2020b). Inverting topography for landscape evolution model process representation: 1. Conceptualization and sensitivity analysis. *Journal of Geophysical Research: Earth Surface*, 125, e2018JF004961. <https://doi.org/10.1029/2018JF004961>
- Barnhart, K. R., Tucker, G. E., Doty, S., Shobe, C. M., Glade, R. C., Rossi, M. W., & Hill, M. C. (2020c). Inverting topography for landscape evolution model process representation: 2. Calibration and validation. *Journal of Geophysical Research: Earth Surface*, 125, e2018JF004963. <https://doi.org/10.1029/2018JF004963>
- Bathurst, J. (2002). At-a-site variation and minimum flow resistance for mountain rivers. *Journal of Hydrology*, 269(1-2), 11–26.
- Beer, A. R., & Turowski, J. M. (2015). Bedload transport controls bedrock erosion under sediment-starved conditions. *Earth Surface Dynamics*, 3(3), 291–309. <https://doi.org/10.5194/esurf-3-291-2015>
- Bennett, S. J. (2017). Report of the West Valley Erosion Working Group Study 2: Recent erosion and deposition processes: Task 2.2: Infiltration and soil moisture determination; Task 2.5: Erodibility of cohesive sediment; Task 2.6: Erodibility of clastic sediment in selected gullies, stream channels, and streambanks. Phase 1 Studies Erosion Working Group. Retrieved from http://www.westvalleyphaseonestudies.org/documents/EWG%20Study%20%20Report_Tasks%202.2%2c%202.5%2c%202.6_5.2.17.pdf
- Berlin, M., & Anderson, R. S. (2007). Modeling of knickpoint retreat on the Roan Plateau, western Colorado. *Journal of Geophysical Research*, 112, F03S06. <https://doi.org/10.1029/2006JF000553>
- Bishop, P. (2007). Long-term landscape evolution: Linking tectonics and surface processes. *Earth Surface Processes and Landforms*, 32, 329–365. <https://doi.org/10.5194/esurf-3-291-2015>
- Blöschl, G., & Sivapalan, M. (1995). Scale issues in hydrological modelling: A review. *Hydrological Processes*, 9(3-4), 251–290. <https://doi.org/10.1002/hyp.3360090305>
- Buffington, J. M., & Montgomery, D. R. (1997). A systematic analysis of eight decades of incipient motion studies, with special reference to gravel-bedded rivers. *Water Resources Research*, 33(8), 1993–2029. <https://doi.org/10.1029/96WR03190>
- Burnham, K. P., & Anderson, D. R. (2003). *Model selection and multimodel inference: A practical information-theoretic approach*. Springer Science & Business Media.
- Carson, M. A., & Kirkby, M. J. (1972). *Hillslope form and processes*. Cambridge: Cambridge University Press.
- Chatanantavet, P., & Parker, G. (2008). Experimental study of bedrock channel alluviation under varied sediment supply and hydraulic conditions. *Water Resources Research*, 44, W12446. <https://doi.org/10.1029/2007WR006581>
- Chen, A., Darbon, J., & Morel, J.-M. (2014). Landscape evolution models: A review of their fundamental equations. *Geomorphology*, 219, 68–86. <https://doi.org/10.1016/j.geomorph.2014.04.037>
- Clapeyron, É. (1834). Mémoire sur la puissance motrice de la chaleur. *Journal de l'École polytechnique*, 14, 153–190.
- Codilean, A. T., Bishop, P., & Hoey, T. B. (2006). Surface process models and the links between tectonics and topography. *Progress in Physical Geography*, 30, 307–333. <https://doi.org/10.1191/0309133306pp480ra>
- Coulthard, T. J. (2001). Landscape evolution models: A software review. *Hydrological Processes*, 15, 165–173. <https://doi.org/10.1002/hyp.426>
- Coulthard, T. J., & Skinner, C. J. (2016). The sensitivity of landscape evolution models to spatial and temporal rainfall resolution. *Earth Surface Dynamics*, 4(3), 757–771. <https://doi.org/10.5194/esurf-4-757-2016>
- Cowie, P. A., Whittaker, A. C., Attal, M., Roberts, G., Tucker, G. E., & Ganas, A. (2008). New constraints on sediment-flux-dependent river incision: Implications for extracting tectonic signals from river profiles. *Geology*, 36(7), 535. <https://doi.org/10.1130/G24681A.1>
- Cox, N. J. (1980). On the relationship between bedrock lowering and regolith thickness. *Earth Surface Processes*, 5(3), 271–274. <https://doi.org/10.1002/esp.3760050305>
- Crosby, B. T., & Whipple, K. X. (2006). Knickpoint initiation and distribution within fluvial networks: 236 waterfalls in the Waipaoa River, North Island, New Zealand. *Geomorphology*, 82(1-2), 16–38. <https://doi.org/10.1016/j.geomorph.2005.08.023>
- Culling, W. (1960). Analytical theory of erosion. *The Journal of Geology*, 68(3), 336–344. Retrieved from <http://www.jstor.org/stable/30059222>
- Culling, W. (1963). Soil creep and the development of hillside slopes. *The Journal of Geology*, 71, 127–161. Retrieved from <http://www.jstor.org/stable/30066150>
- Culling, W. (1965). Theory of erosion on soil-covered slopes. *The Journal of Geology*, 73(2), 230–254. Retrieved from <https://www.jstor.org/stable/>
- DOE, & NYSERDA (2010). Final environmental impact statement for decommissioning and/or long-term stewardship at the West Valley Demonstration Project and western New York Nuclear Service Center (doe/eis-0226), United States Department of Energy and New York State Energy Research and Development Authority. https://www.energy.gov/sites/prod/files/EIS-0226-FEIS_Vol2-2010.pdf
- Dai, A. (2013). Increasing drought under global warming in observations and models. *Nature Climate Change*, 3(1), 52. <https://doi.org/10.1038/nclimate1633>
- Davis, W. (1892). The convex profile of bad-land divides. *Science (New York, NY)*, 20(508), 245. <https://doi.org/10.1126/science.ns-20.508.245>
- Deal, E., Braun, J., & Botter, G. (2018). Understanding the role of rainfall and hydrology in determining fluvial erosion efficiency. *Journal of Geophysical Research: Earth Surface*, 123, 744–778. <https://doi.org/10.1002/2017JF004393>
- Densmore, A. L., Ellis, M. A., & Anderson, R. S. (1998). Landsliding and the evolution of normal-fault-bounded mountains. *Journal of Geophysical Research*, 103(B7), 15,203–15,219. <https://doi.org/10.1029/98JB00510>
- DiBiase, R. A., & Whipple, K. X. (2011). The influence of erosion thresholds and runoff variability on the relationships among topography, climate, and erosion rate. *Journal of Geophysical Research*, 116, F04036. <https://doi.org/10.1029/2011JF002095>
- Dietrich, W. E., Bellugi, D. G., Sklar, L. S., Stock, J. D., Heimsath, A. M., & Roering, J. J. (2003). Geomorphic transport laws for predicting landscape form and dynamics. In P. Wilcock, & R. Iverson (Eds.), *Prediction in geomorphology*, Geophysical Monograph Series. Washington, DC: AGU. <https://doi.org/10.1029/135GM09>
- Dunne, T., & Leopold, L. B. (1978). *Water in environmental planning*: Macmillan.

- Eagleson, P. S. (1978). Climate, soil, and vegetation: 2. The distribution of annual precipitation derived from observed storm sequences. *Water Resources Research*, *14*, 713–721. <https://doi.org/10.1029/WR014i005p00713>
- Einstein, H. A. (1950). The bed-load function for sediment transportation in open channel flows (Tech. Rep. No. 1026). Washington, D.C., USA: United States Department of Agriculture, Soil Conservation Service.
- Fakundiny, R. (1985). Practical applications of geological methods at the West Valley low-level radioactive waste burial ground, western New York. *Northeastern Environmental Science*, *4*(3-4), 116–148.
- Ferguson, R. I., Sharma, B. P., Hodge, R. A., Hardy, R. J., & Warburton, J. (2017). Bed load tracer mobility in a mixed bedrock/alluvial channel. *Journal of Geophysical Research: Earth Surface*, *122*, 807–822. <https://doi.org/10.1002/2016JF003946>
- Finnegan, N. J., Hallet, B., Montgomery, D. R., Zeitler, P. K., Stone, J. O., Anders, A. M., & Yuping, L. (2008). Coupling of rock uplift and river incision in the Namche Barwa-Gyala Peri massif, Tibet. *GSA Bulletin*, *120*(1-2), 142–155. <https://doi.org/10.1130/B26224.1>
- Finnegan, N. J., Sklar, L. S., & Fuller, T. K. (2007). Interplay of sediment supply, river incision, and channel morphology revealed by the transient evolution of an experimental bedrock channel. *Journal of Geophysical Research*, *112*, F03S11. <https://doi.org/10.1029/2006JF000569>
- Flanagan, D. C., Ascough, J. C., Nearing, M. A., & Laflen, J. M. (2001). The Water Erosion Prediction Project (WEPP) model. In R. S. Harmon, & W. W. Doe (Eds.), *Landscape erosion and evolution modeling* (pp. 145–199). Boston, MA: Springer US. https://doi.org/10.1007/978-1-4615-0575-4_7
- Foley, M. G. (1980). Bed-rock incision by streams. *GSA Bulletin*, *91*(10 Part II), 2189–2213. <https://doi.org/10.1130/GSAB-P2-91-2189>
- Furbish, D. J., Haff, P. K., Dietrich, W. E., & Heimsath, A. M. (2009). Statistical description of slope-dependent soil transport and the diffusion-like coefficient. *Journal of Geophysical Research*, *114*, F00A05. <https://doi.org/10.1029/2009JF001267>
- Ganti, V., Passalacqua, P., & Fofoula-Georgiou, E. (2012). A sub-grid scale closure for nonlinear hillslope sediment transport models. *Journal of Geophysical Research*, *117*, F02012. <https://doi.org/10.1029/2011JF002181>
- García-Castellanos, D., & O'Connor, J. E. (2018). Outburst floods provide erodability estimates consistent with long-term landscape evolution. *Scientific Reports*, *8*, 10573. <https://doi.org/10.1038/s41598-018-28981-y>
- Gasparini, N. M., & Brandon, M. T. (2011). A generalized power law approximation for fluvial incision of bedrock channels. *Journal of Geophysical Research*, *116*, F02020. <https://doi.org/10.1029/2009JF001655>
- Gasparini, N. M., Bras, R. L., & Whipple, K. X. (2006). Numerical modeling of non-steady-state river profile evolution using a sediment-flux-dependent incision model. *Special Paper of the Geological Society of America*, *398*, 127–141. [https://doi.org/10.1130/2006.2398\(08\)](https://doi.org/10.1130/2006.2398(08))
- Gasparini, N. M., Tucker, G., & Bras, R. (2004). Network-scale dynamics of grain-size sorting: Implications for downstream fining, stream-profile concavity, and drainage basin morphology. *Earth Surface Processes and Landforms*, *29*(4), 401–421. <https://doi.org/10.1002/esp.1031>
- Gentile, P., Troy, T. J., Lintner, B. R., & Findell, K. L. (2012). Scaling in surface hydrology: Progress and challenges. *Journal of Contemporary Water Research & Education*, *147*(1), 28–40. <https://doi.org/10.1111/j.1936-704X.2012.03105.x>
- Gilbert, G. (1877). Report on the geology of the Henry Mountains: US Geog. and Geol. Survey, Rocky Mtn. Region, 160. <https://doi.org/10.3133/70039916>
- Giorgi, F., Im, E.-S., Coppola, E., Diffenbaugh, N., Gao, X., Mariotti, L., & Shi, Y. (2011). Higher hydroclimatic intensity with global warming. *Journal of Climate*, *24*(20), 5309–5324. <https://doi.org/10.1175/2011JCLI3979.1>
- Gleason, C. J. (2015). Hydraulic geometry of natural rivers. *Progress in Physical Geography*, *39*(3), 337–360. <https://doi.org/10.1177/0309133314567584>
- Gran, K. B., Finnegan, N., Johnson, A. L., Belmont, P., Wittkop, C., & Rittenour, T. (2013). Landscape evolution, valley excavation, and terrace development following abrupt postglacial base-level fall. *Geological Society of America Bulletin*, *125*(11-12), 1851–1864. <https://doi.org/10.1130/B30772.1>
- Grieve, S. W. D., Mudd, S. M., & Hurst, M. D. (2016). How long is a hillslope? *Earth Surface Processes and Landforms*, *41*(8), 1039–1054. <https://doi.org/10.1002/esp.3884>
- Grieve, S. W. D., Mudd, S. M., Hurst, M. D., & Milodowski, D. T. (2016). A nondimensional framework for exploring the relief structure of landscapes. *Earth Surface Dynamics*, *4*(2), 309–325. <https://doi.org/10.5194/esurf-4-309-2016>
- Gupta, V. K., Rodríguez-Iturbe, I., & Wood, E. F. (1986). *Scale problems in hydrology: Runoff generation and basin response* (Vol. 6). Springer Science & Business Media. <https://doi.org/10.1007/978-94-009-4678-1>
- Hack, J. T. (1957). Studies of longitudinal stream profiles in Virginia and Maryland. U.S. Geological Survey Professional Paper 294-B. <https://doi.org/10.3133/pp294B>
- Hancock, G. S., & Anderson, R. S. (2002). Numerical modeling of fluvial strath-terrace formation in response to oscillating climate. *Geological Society of America Bulletin*, *114*(9), 1131–1142. [https://doi.org/10.1130/0016-7606\(2002\)114<1131:NMOFST>2.0.CO;2](https://doi.org/10.1130/0016-7606(2002)114<1131:NMOFST>2.0.CO;2)
- Hancock, G. R., Coulthard, T. J., Martinez, C., & Kalma, J. D. (2011). An evaluation of landscape evolution models to simulate decadal and centennial scale soil erosion in grassland catchments. *Journal of Hydrology*, *398*(3-4), 171–183. <https://doi.org/10.1016/j.jhydrol.2010.12.002>
- Hancock, G. R., Evans, K., Willgoose, G. R., Moliere, D., Saynor, M., & Loch, R. (2000). Medium-term erosion simulation of an abandoned mine site using the SIBERIA landscape evolution model. *Australian Journal of Soil Research*, *38*(2), 249–264. <https://doi.org/10.1071/SR99035>
- Hancock, G. R., Lowry, J., Coulthard, T. J., Evans, K., & Moliere, D. (2010). A catchment scale evaluation of the SIBERIA and CAESAR landscape evolution models. *Earth Surface Processes and Landforms*, *35*(8), 863–875. <https://doi.org/10.1002/esp.1863>
- Hancock, G. R., Wells, T., Dever, C., & Braggins, M. (2018). Hillslope and point based soil erosion—An evaluation of a Landscape Evolution Model. *Earth Surface Processes and Landforms*, *44*(5), 1163–1177. <https://doi.org/10.1002/esp.4566>
- Hancock, G. R., & Willgoose, G. R. (2001). Use of a landscape simulator in the validation of the SIBERIA catchment evolution model: Declining equilibrium landforms. *Water Resources Research*, *37*(7), 1981–1992. <https://doi.org/10.1029/2001WR900002>
- Hanks, T. C. (2000). The age of scarplike landforms from diffusion-equation analysis. *Quaternary Geochronology: Methods and Applications*, *4*, 313–338. <https://doi.org/10.1029/RF004p0313>
- Hanks, T. C., Bucknam, R. C., Lajoie, K. R., & Wallace, R. E. (1984). Modification of wave-cut and faulting-controlled landforms. *Journal of Geophysical Research*, *89*(B7), 5771–5790. <https://doi.org/10.1029/JB089iB07p05771>
- Harel, M. A., Mudd, S. M., & Attal, M. (2016). Global analysis of the stream power law parameters based on worldwide ¹⁰Be denudation rates. *Geomorphology*, *268*, 184–196. <https://doi.org/10.1016/j.geomorph.2016.05.035>
- Heimsath, A. M., Chappell, J., Dietrich, W. E., Nishiizumi, K., & Finkel, R. C. (2001). Late Quaternary erosion in Southeastern Australia: A field example using cosmogenic nuclides. *Quaternary International*, *83*, 169–185. [https://doi.org/10.1016/S1040-6182\(01\)00038-6](https://doi.org/10.1016/S1040-6182(01)00038-6)

- Heimsath, A. M., Dietrich, W. E., Nishiizumi, K., & Finkel, R. C. (1997). The soil production function and landscape equilibrium. *Nature*, 388(6640), 358–361. <https://doi.org/10.1038/41056>
- Heimsath, A. M., Dietrich, W. E., Nishiizumi, K., & Finkel, R. C. (1999). Cosmogenic nuclides, topography, and the spatial variation of soil depth. *Geomorphology*, 27(1), 151–172. [https://doi.org/10.1016/S0169-555X\(98\)00095-6](https://doi.org/10.1016/S0169-555X(98)00095-6)
- Heimsath, A. M., Dietrich, W. E., Nishiizumi, K., & Finkel, R. C. (2001). Stochastic processes of soil production and transport: Erosion rates, topographic variation and cosmogenic nuclides in the Oregon Coast range. *Earth Surface Processes and Landforms*, 26(5), 531–552. <https://doi.org/10.1002/esp.209>
- Heimsath, A. M., Fink, D., & Hancock, G. R. (2009). The ‘humped’ soil production function: Eroding Arnhem Land, Australia. *Earth Surface Processes and Landforms*, 34(12), 1674–1684. <https://doi.org/10.1002/esp.1859>
- Hill, M. C., & Tiedeman, C. R. (2007). *Effective groundwater model calibration: With analysis of data, sensitivities, predictions, and uncertainty*. John Wiley. <https://doi.org/10.1002/0470041080>
- Hobley, D. E., Sinclair, H. D., Mudd, S. M., & Cowie, P. A. (2011). Field calibration of sediment flux dependent river incision. *Journal of Geophysical Research*, 116, F04017. <https://doi.org/10.1029/2010JF001935>
- Howard, A. D. (1980). Thresholds in river regimes. *Thresholds in geomorphology*, 227, 227–258.
- Howard, A. D. (1994). A detachment-limited model of drainage basin evolution. *Water Resources Research*, 30(7), 2261–2285. <https://doi.org/10.1029/94WR00757>
- Howard, A. D., Dietrich, W. E., & Seidl, M. A. (1994). Modeling fluvial erosion on regional to continental scales. *Journal of Geophysical Research*, 99(B7), 13,971–13,986. <https://doi.org/10.1029/94JB00744>
- Howard, A. D., & Kerby, G. (1983). Channel changes in badlands. *Geological Society of America Bulletin*, 94, 739–752. [https://doi.org/10.1130/0016-7606\(1983\)94<739:CCIB>2.0.CO;2](https://doi.org/10.1130/0016-7606(1983)94<739:CCIB>2.0.CO;2)
- Huang, X., & Niemann, J. D. (2006). Modelling the potential impacts of groundwater hydrology on long-term drainage basin evolution. *Earth Surface Processes and Landforms*, 31(14), 1802–1823. <https://doi.org/10.1002/esp.1369>
- Huang, X., & Niemann, J. D. (2008). How do streamflow generation mechanisms affect watershed hypsometry? *Earth Surface Processes and Landforms*, 33(5), 751–772. <https://doi.org/10.1002/esp.1573>
- Hunt, A. G. (2015). Soil depth and soil production. *Complexity*, 21(6), 42–49. <https://doi.org/10.1002/cplx.21664>
- Hunt, A. G., & Ghanbarian, B. (2016). Percolation theory for solute transport in porous media: Geochemistry, geomorphology, and carbon cycling. *Water Resources Research*, 52, 7444–7459. <https://doi.org/10.1002/2016WR019289>
- Inoue, T., Izumi, N., Shimizu, Y., & Parker, G. (2014). Interaction among alluvial cover, bed roughness, and incision rate in purely bedrock and alluvial-bedrock channel. *Journal of Geophysical Research: Earth Surface*, 119, 2123–2146. <https://doi.org/10.1002/2014JF003133>
- Johnson, J. P. L. (2016). Gravel threshold of motion: A state function of sediment transport disequilibrium? *Earth Surface Dynamics*, 4(3), 685–703. <https://doi.org/10.5194/esurf-4-685-2016>
- Johnson, J. P. L., & Whipple, K. X. (2007). Feedbacks between erosion and sediment transport in experimental bedrock channels. *Earth Surface Processes and Landforms*, 32(7), 1048–1062. <https://doi.org/10.1002/esp.1471>
- Johnson, J. P. L., & Whipple, K. X. (2010). Evaluating the controls of shear stress, sediment supply, alluvial cover, and channel morphology on experimental bedrock incision rate. *Journal of Geophysical Research*, 115, F02018. <https://doi.org/10.1029/2009JF001335>
- Johnson, J. P. L., Whipple, K. X., & Sklar, L. S. (2010). Contrasting bedrock incision rates from snowmelt and flash floods in the Henry Mountains, Utah. *GSA Bulletin*, 122(9-10), 1600–1615. <https://doi.org/10.1130/B30126.1>
- Johnson, J. P. L., Whipple, K. X., Sklar, L. S., & Hanks, T. C. (2009). Transport slopes, sediment cover, and bedrock channel incision in the Henry Mountains, Utah. *Journal of Geophysical Research*, 114, W12446. <https://doi.org/10.1029/2007JF000862>
- Kirchner, J. W. (2006). Getting the right answers for the right reasons: Linking measurements, analyses, and models to advance the science of hydrology. *Water Resources Research*, 42, W03S04. <https://doi.org/10.1029/2005WR004362>
- Kirkby, M. J. (1969). Erosion by water on hillslopes. *Water, earth and man* (pp. 229–238).
- Kirkby, M. J. (1994). Thresholds and instability in stream head hollows: A model of magnitude and frequency for wash processes. *Process models and theoretical geomorphology* (pp. 149–159). Chichester: Wiley.
- Kirkby, M. J., Abraham, R., McMahon, M. D., Shao, J., & Thornes, J. B. (1998). MEDALUS soil erosion models for global change. *Geomorphology*, 24(1), 35–49. [https://doi.org/10.1016/S0169-555X\(97\)00099-8](https://doi.org/10.1016/S0169-555X(97)00099-8)
- Kirkby, M. J., & Cox, N. J. (1995). A climatic index for soil erosion potential (CSEP) including seasonal and vegetation factors. *Catena*, 25(1), 333–352. [https://doi.org/10.1016/0341-8162\(95\)00016-L](https://doi.org/10.1016/0341-8162(95)00016-L)
- Klemes, V. (1983). Conceptualization and scale in hydrology. *Journal of Hydrology*, 65, 1–23. [https://doi.org/10.1016/0022-1694\(83\)90208-1](https://doi.org/10.1016/0022-1694(83)90208-1)
- Lague, D. (2013). The stream power river incision model: Evidence, theory and beyond. *Earth Surface Processes and Landforms*, 39(1), 38–61. <https://doi.org/10.1002/esp.3462>
- Lague, D., Hovius, N., & Davy, P. (2005). Discharge, discharge variability, and the bedrock channel profile. *Journal of Geophysical Research*, 110, F04006. <https://doi.org/10.1029/2004JF000259>
- Laherrere, J., & Sornette, D. (1998). Stretched exponential distributions in nature and economy: fat tails with characteristic scales. *The European Physical Journal B-Condensed Matter and Complex Systems*, 2(4), 525–539.
- Lamb, M. P., Dietrich, W. E., & Sklar, L. S. (2008). A model for fluvial bedrock incision by impacting suspended and bed load sediment. *Journal of Geophysical Research*, 113, F03025. <https://doi.org/10.1029/2007JF000915>
- Lamb, M. P., Dietrich, W. E., & Venditti, J. G. (2008). Is the critical Shields stress for incipient sediment motion dependent on channel-bed slope? *Journal of Geophysical Research*, 113, F02008. <https://doi.org/10.1029/2007JF000831>
- Langston, A. L., & Tucker, G. E. (2018). Developing and exploring a theory for the lateral erosion of bedrock channels for use in landscape evolution models. *Earth Surface Dynamics*, 6(1), 1–27. <https://doi.org/10.5194/esurf-6-1-2018>
- Lau, W. K.-M., Wu, H.-T., & Kim, K.-M. (2013). A canonical response of precipitation characteristics to global warming from CMIP5 models. *Geophysical Research Letters*, 40, 3163–3169. <https://doi.org/10.1002/grl.50420>
- Lavé, J., & Avouac, J. P. (2001). Fluvial incision and tectonic uplift across the Himalayas of central Nepal. *Journal of Geophysical Research*, 106(B11), 26,561–26,591. <https://doi.org/10.1029/2001JB000359>
- Leopold, L. B., & Maddock, T. (1953). The hydraulic geometry of stream channels and some physiographic implications. United States Geological Survey Professional Paper 252. <https://doi.org/10.3133/pp252>
- Leopold, L. B., & Miller, J. P. (1956). *Ephemeral streams: Hydraulic factors and their relation to the drainage net* (Vol. 282). US Government Printing Office. <https://doi.org/10.3133/pp282A>
- Martin, Y., & Church, M. (2004). Numerical modelling of landscape evolution: Geomorphological perspectives. *Progress in Physical Geography*, 28, 317–339. <https://doi.org/10.1191/0309133304pp412ra>

- Masteller, C. C., Finnegan, N. J., Turowski, J. M., Yager, E. M., & Rickenmann, D. (2019). History dependent threshold for motion revealed by continuous bedload transport measurements in a steep mountain stream. *Geophysical Research Letters*, *46*, 2583–2591. <https://doi.org/10.1029/2018GL081325>
- McDonnell, J. J., Sivapalan, M., Vaché, K., Dunn, S., Grant, G., Haggerty, R., et al. (2007). Moving beyond heterogeneity and process complexity: A new vision for watershed hydrology. *Water Resources Research*, *43*, W07301. <https://doi.org/10.1029/2006WR005467>
- McKean, J. A., Dietrich, W. E., Finkel, R. C., Southon, J. R., & Caffee, M. W. (1993). Quantification of soil production and downslope creep rates from cosmogenic ¹⁰Be accumulations on a hillslope profile. *Geology*, *21*(4), 343–346. [https://doi.org/10.1130/0091-7613\(1993\)021<0343:QOSPAD>2.3.CO;2](https://doi.org/10.1130/0091-7613(1993)021<0343:QOSPAD>2.3.CO;2)
- Menne, M. J., Durre, I., Vose, R. S., Gleason, B. E., & Houston, T. G. (2012). An overview of the global historical climatology network-daily database. *Journal of Atmospheric and Oceanic Technology*, *29*(7), 897–910. <https://doi.org/10.1175/JTECH-D-11-00103.1>
- Meyer-Peter, E., & Müller, R. (1948). Formulas for bed-load transport, IAHR. IaHR 2nd meeting, Stockholm, Appendix 2.
- Mohanty, B., Kanwar, R. S., & Everts, C. (1994). Comparison of saturated hydraulic conductivity measurement methods for a glacial-till soil. *Soil Science Society of America Journal*, *58*(3), 672–677. <https://doi.org/10.2136/sssaj1994.03615995005800030006x>
- Molieri, D., Evans, K., & Willgoose, G. R. (2002). Temporal trends in erosion and hydrology for a post-mining landform at ranger mine. Supervising Scientist Report 165.
- Molnar, P. (2001). Climate change, flooding in arid environments, and erosion rates. *Geology*, *29*(12), 1071–1074. [https://doi.org/10.1130/0091-7613\(2001\)029<1071:CCFIAE>2.0.CO;2](https://doi.org/10.1130/0091-7613(2001)029<1071:CCFIAE>2.0.CO;2)
- Narteau, C., Zhang, D., Rozier, O., & Claudin, P. (2009). Setting the length and time scales of a cellular automaton dune model from the analysis of superimposed bed forms. *Journal of Geophysical Research*, *114*, F03006. <https://doi.org/10.1029/2008JF001127>
- Nash, D. B. (1980). Morphologic dating of degraded normal fault scarps. *The Journal of Geology*, *88*(3), 353–360. Retrieved from <https://www.jstor.org/stable/30062456>
- O’Gorman, P. A., & Schneider, T. (2009). The physical basis for increases in precipitation extremes in simulations of 21st-century climate change. *Proceedings of the National Academy of Sciences*, *106*(35), 14,773–14,777. <https://doi.org/10.1073/pnas.0907610106>
- Passalacqua, P., Port-Agel, F., Foufoula-Georgiou, E., & Paola, C. (2006). Application of dynamic subgrid-scale concepts from large-eddy simulation to modeling landscape evolution. *Water Resources Research*, *42*, W06D11. <https://doi.org/10.1029/2006WR004879>
- Pazzaglia, F. J. (2003). Landscape evolution models. *Developments in Quaternary Sciences*, *1*, 247–274. [https://doi.org/10.1016/S1571-0866\(03\)01012-1](https://doi.org/10.1016/S1571-0866(03)01012-1)
- Pelletier, J. D. (2010). Minimizing the grid-resolution dependence of flow-routing algorithms for geomorphic applications. *Geomorphology*, *122*(1–2), 91–98. <https://doi.org/10.1016/j.geomorph.2010.06.001>
- Pelletier, J. D. (2013). 2.3 Fundamental principles and techniques of landscape evolution modeling. *Treatise on geomorphology* (pp. 29–43). San Diego: Elsevier. <https://doi.org/10.1016/B978-0-12-374739-6.00025-7>
- Pelletier, J. D., DeLong, S. B., Al-Suwaidi, A. H., Cline, M., Lewis, Y., Psillas, J. L., & Yanites, B. (2006). Evolution of the Bonneville shoreline scarp in west-central Utah: Comparison of scarp-analysis methods and implications for the diffusion model of hillslope evolution. *Geomorphology*, *74*, 257–270. <https://doi.org/10.1016/j.geomorph.2005.08.008>
- Pepin, E., Carretier, S., & Hérail, G. (2010). Erosion dynamics modelling in a coupled catchment–fan system with constant external forcing. *Geomorphology*, *122*(1), 78–90. <https://doi.org/10.1016/j.geomorph.2010.04.029>
- Perron, J. T., Dietrich, W. E., & Kirchner, J. W. (2008). Controls on the spacing of first-order valleys. *Journal of Geophysical Research*, *113*, F04016. <https://doi.org/10.1029/2007JF000977>
- Petit, C., Gunnell, Y., Saholiariliva, N. G., Meyer, B., & Séguinot, J. (2009). Faceted spurs at normal fault scarps: Insights from numerical modeling. *Journal of Geophysical Research*, *114*, B05403. <https://doi.org/10.1029/2008JB005955>
- Pfister, L., & Kirchner, J. W. (2017). Debates–hypothesis testing in hydrology: Theory and practice. *Water Resources Research*, *53*, 1792–1798. <https://doi.org/10.1002/2016WR020116>
- Portenga, E. W., & Bierman, P. R. (2011). Understanding earth’s eroding surface with ¹⁰Be. *GSA Today*, *21*(8), 4–10. <https://doi.org/10.1130/G111A.1>
- Prancevic, J. P., & Lamb, M. P. (2015). Unraveling bed slope from relative roughness in initial sediment motion. *Journal of Geophysical Research: Earth Surface*, *120*, 474–489. <https://doi.org/10.1002/2014JF003323>
- Prancevic, J. P., Lamb, M. P., & Fuller, B. M. (2014). Incipient sediment motion across the river to debris-flow transition. *Geology*, *42*(3), 191–194. <https://doi.org/10.1130/g34927.1>
- Prosser, I. P., & Rustomji, P. (2000). Sediment transport capacity relations for overland flow. *Progress in Physical Geography*, *24*(2), 179–193. <https://doi.org/10.1177/030913330002400202>
- Richardson, P. W., Perron, J. T., & Schurr, N. D. (2019). Influences of climate and life on hillslope sediment transport. *Geology*, *47*(5), 423–426. <https://doi.org/10.1130/G45305.1>
- Riggins, S. G., Anderson, R. S., Anderson, S. P., & Tye, A. M. (2011). Solving a conundrum of a steady-state hilltop with variable soil depths and production rates, Bodmin Moor, UK. *Geomorphology*, *128*(1), 73–84. <https://doi.org/10.1016/j.geomorph.2010.12.023>
- Rodríguez-Iturbe, I., & Rinaldo, A. (2001). *Fractal river basins: chance and self-organization*. Cambridge: Cambridge University Press.
- Roering, J. J. (2008). How well can hillslope evolution models “explain” topography? Simulating soil transport and production with high-resolution topographic data. *Geological Society of America Bulletin*, *120*(9–10), 1248–1262. <https://doi.org/10.1130/B26283.1>
- Roering, J., Kirchner, J., & Dietrich, W. E. (1999). Evidence for nonlinear, diffusive sediment transport on hillslopes and implications for landscape morphology. *Water Resources Research*, *35*(3), 853–870. <https://doi.org/10.1029/1998WR900090>
- Roering, J., Kirchner, J., Sklar, L., & Dietrich, W. E. (2001). Hillslope evolution by nonlinear creep and landsliding: An experimental study. *Geology*, *29*(2), 143–146. [https://doi.org/10.1130/0091-7613\(2001\)029<0143:HEBNCA>2.0.CO;2](https://doi.org/10.1130/0091-7613(2001)029<0143:HEBNCA>2.0.CO;2)
- Roering, J. J., Perron, J. T., & Kirchner, J. W. (2007). Functional relationships between denudation and hillslope form and relief. *Earth and Planetary Science Letters*, *264*(1), 245–258. <https://doi.org/10.1016/j.epsl.2007.09.035>
- Ronayne, M. J., Houghton, T. B., & Stednick, J. D. (2012). Field characterization of hydraulic conductivity in a heterogeneous alpine glacial till. *Journal of Hydrology*, *458*, 103–109. <https://doi.org/10.1016/j.jhydrol.2012.06.036>
- Rosenbloom, N. A., & Anderson, R. S. (1994). Hillslope and channel evolution in a marine terraced landscape, Santa Cruz, California. *Journal of Geophysical Research*, *99*, 14,013–14,029. <https://doi.org/10.1029/94JB00048>
- Rossi, M. W., Whipple, K. X., & Vivoni, E. R. (2016). Precipitation and evapotranspiration controls on daily runoff variability in the contiguous United States and Puerto Rico. *Journal of Geophysical Research: Earth Surface*, *121*, 128–145. <https://doi.org/10.1002/2015JF003446>
- Russo, D., & Bresler, E. (1981). Soil hydraulic properties as stochastic processes: I. An analysis of field spatial variability. *Soil Science Society of America Journal*, *45*(4), 682–687. <https://doi.org/10.2136/sssaj1981.03615995004500040002x>

- Schoorl, J., Sonneveld, M. P. W., & Veldkamp, A. (2000). Three-dimensional landscape process modelling: The effect of DEM resolution. *Earth Surface Processes and Landforms*, 25(9), 1025–1034. [https://doi.org/10.1002/1096-9837\(200008\)25:9<1025::AID-ESP116>3.0.CO;2-Z](https://doi.org/10.1002/1096-9837(200008)25:9<1025::AID-ESP116>3.0.CO;2-Z)
- Seidl, M. A., & Dietrich, W. E. (1992). The problem of channel erosion into bedrock. *Catena supplement*, 23, 101–124.
- Seidl, M. A., Dietrich, W. E., & Kirchner, J. W. (1994). Longitudinal profile development into bedrock: An analysis of Hawaiian channels. *The Journal of Geology*, 102(4), 457–474. Retrieved from <https://www.jstor.org/stable/30065663>
- Shepherd, R. G. (1972). Incised river meanders: Evolution in simulated bedrock. *Science*, 178(4059), 409–411. <https://doi.org/10.1126/science.178.4059.409>
- Shepherd, R. G., & Schumm, S. A. (1974). Experimental study of river incision. *GSA Bulletin*, 85(2), 257–268. [https://doi.org/10.1130/0016-7606\(1974\)85<257:ESORI>2.0.CO;2](https://doi.org/10.1130/0016-7606(1974)85<257:ESORI>2.0.CO;2)
- Sivapalan, M. (2003). Process complexity at hillslope scale, process simplicity at the watershed scale: Is there a connection? *Hydrological Processes*, 17(5), 1037–1041. <https://doi.org/10.1002/hyp.5109>
- Sklar, L., & Dietrich, W. E. (1998). River longitudinal profiles and bedrock incision models: Stream power and the influence of sediment supply. *Geophysical Monograph-American Geophysical Union*, 107, 237–260. <https://doi.org/10.1029/GM107p0237>
- Sklar, L. S., & Dietrich, W. E. (2001). Sediment and rock strength controls on river incision into bedrock. *Geology*, 29(12), 1087–1090. [https://doi.org/10.1130/0091-7613\(2001\)029<1087:SARSCO>2.0.CO;2](https://doi.org/10.1130/0091-7613(2001)029<1087:SARSCO>2.0.CO;2)
- Sklar, L. S., & Dietrich, W. E. (2004). A mechanistic model for river incision into bedrock by saltating bed load. *Water Resources Research*, 40, W06301. <https://doi.org/10.1029/2003WR002496>
- Sklar, L., & Dietrich, W. E. (2006). The role of sediment in controlling steady-state bedrock channel slope: Implications of the saltation-abrasion incision model. *Geomorphology*, 82(1-2), 58–83. <https://doi.org/10.1016/j.geomorph.2005.08.019>
- Slingerland, R. L., Furlong, K., & Harbaugh, J. (1994). *Simulating clastic sedimentary basins: Physical fundamentals and computing procedures*: Prentice Hall.
- Small, E. E., Anderson, R. S., & Hancock, G. S. (1999). Estimates of the rate of regolith production using ¹⁰Be and ²⁶Al from an alpine hillslope. *Geomorphology*, 27(1), 131–150. [https://doi.org/10.1016/S0169-555X\(98\)00094-4](https://doi.org/10.1016/S0169-555X(98)00094-4)
- Smith, T. R., & Bretherton, F. P. (1972). Stability and the conservation of mass in drainage basin evolution. *Water Resources Research*, 8(6), 1506–1529. <https://doi.org/10.1029/WR008i006p01506>
- Snow, R. S., & Slingerland, R. (1987). Mathematical modeling of graded river profiles. *Journal of Geology*, 95, 15–33. Retrieved from <https://www.jstor.org/stable/30081066>
- Snyder, N. P., Whipple, K. X., Tucker, G. E., & Merritts, D. J. (2003). Channel response to tectonic forcing: Field analysis of stream morphology and hydrology in the Mendocino Triple Junction Region, Northern California. *Geomorphology*, 53(1-2), 97–127. [https://doi.org/10.1016/S0169-555X\(02\)00349-5](https://doi.org/10.1016/S0169-555X(02)00349-5)
- Sólyom, P. B., & Tucker, G. E. (2004). Effect of limited storm duration on landscape evolution, drainage basin geometry, and hydrograph shapes. *Journal of Geophysical Research*, 109, F03012. <https://doi.org/10.1029/2003JF000032>
- Stock, J. D., & Montgomery, D. R. (1999). Geologic constraints on bedrock river incision using the stream power law. *Journal of Geophysical Research*, 104, 4983–4993. <https://doi.org/10.1029/98JB02139>
- Stockmann, U., Minasny, B., & McBratney, A. B. (2014). How fast does soil grow? *Geoderma*, 216, 48–61. <https://doi.org/10.1016/j.geoderma.2013.10.007>
- Strobel, M. L. (1993). Hydraulic properties of three types of glacial deposits in Ohio. US Geological Survey; Books and Open-File Reports Section. <https://doi.org/10.3133/wri924135>
- Taylor, K. E., Stouffer, R. J., & Meehl, G. A. (2012). An overview of CMIP5 and the experiment design. *Bulletin of the American Meteorological Society*, 93(4), 485–498. <https://doi.org/10.1175/BAMS-D-11-00094.1>
- Temme, A., Schoorl, J., Claessens, L., Veldkamp, A., & Shroder, F. (2013). 2.13 Quantitative modeling of landscape evolution. In J. F. Shroder (Ed.), *Treatise on geomorphology* (pp. 180–200). San Diego: Academic Press. <https://doi.org/10.1016/B978-0-12-374739-6.00039-7>
- Tofelde, S., Savi, S., Wickert, A. D., Bufe, A., & Schildgen, T. F. (2019). Alluvial channel response to environmental perturbations: Fill-terrace formation and sediment-signal disruption. *Earth Surface Dynamics*, 7(2), 609–631. <https://doi.org/10.5194/esurf-7-609-2019>
- Tomkin, J. H., Brandon, M. T., Pazzaglia, F. J., Barbour, J. R., & Willett, S. D. (2003). Quantitative testing of bedrock incision models for the Clearwater River, NW Washington State. *Journal of Geophysical Research*, 108, 2308. <https://doi.org/10.1029/2001JB000862>
- Trenberth, K. E. (2011). Changes in precipitation with climate change. *Climate Research*, 47(1/2), 123–138. <https://doi.org/10.3354/cr00953>
- Tucker, G. E. (2004). Drainage basin sensitivity to tectonic and climatic forcing: Implications of a stochastic model for the role of entrainment and erosion thresholds. *Earth Surface Processes and Landforms*, 29(2), 185–205. <https://doi.org/10.1002/esp.1020>
- Tucker, G. E. (2009). Natural experiments in landscape evolution. *Earth Surface Processes and Landforms*, 34, 1450–1460. <https://doi.org/10.1002/esp.1833>
- Tucker, G. E., Arnold, L., Bras, R. L., Flores, H., Istanbuloglu, E., & Sólyom, P. (2006). Headwater channel dynamics in semiarid rangelands, Colorado High Plains, USA. *GSA Bulletin*, 118(7-8), 959–974. <https://doi.org/10.1130/B25928.1>
- Tucker, G. E., & Bras, R. L. (2000). A stochastic approach to modeling the role of rainfall variability in drainage basin evolution. *Water Resources Research*, 36(7), 1953–1964. <https://doi.org/10.1029/2000WR900065>
- Tucker, G. E., & Hancock, G. R. (2010). Modelling landscape evolution. *Earth Surface Processes and Landforms*, 46, 28–50. <https://doi.org/10.1002/esp.1952>
- Tucker, G. E., McCoy, S. W., & Hobbey, D. E. J. (2018). A lattice grain model of hillslope evolution. *Earth Surface Dynamics*, 6(3), 563–582. <https://doi.org/10.5194/esurf-6-563-2018>
- Tucker, G. E., & Slingerland, R. L. (1997). Drainage basin response to climate change. *Water Resources Research*, 33, 2031–2047. <https://doi.org/10.1029/97WR00409>
- Tucker, G. E., & Whipple, K. (2002). Topographic outcomes predicted by stream erosion models: Sensitivity analysis and intermodel comparison. *Journal of Geophysical Research*, 107(B9), 2179. <https://doi.org/10.1029/2001JB000162>
- Turowski, J. M., Hovius, N., Meng-Long, H., Lague, D., & Men-Chiang, C. (2008). Distribution of erosion across bedrock channels. *Earth Surface Processes and Landforms*, 33(3), 353–363. <https://doi.org/10.1002/esp.1559>
- Turowski, J. M., Lague, D., & Hovius, N. (2007). Cover effect in bedrock abrasion: A new derivation and its implications for the modeling of bedrock channel morphology. *Journal of Geophysical Research*, 112, F04006. <https://doi.org/10.1029/2006JF000697>
- Turowski, J. M., & Rickenmann, D. (2009). Tools and cover effects in bedload transport observations in the Pitzbach, Austria. *Earth Surface Processes and Landforms*, 34(1), 26–37. <https://doi.org/10.1002/esp.1686>
- Valla, P. G., van der Beek, P. A., & Lague, D. (2010). Fluvial incision into bedrock: Insights from morphometric analysis and numerical modeling of gorges incising glacial hanging valleys (Western Alps, France). *Journal of Geophysical Research*, 115, F02010. <https://doi.org/10.1029/2008JF001079>

- Valters, D. (2016). Modelling geomorphic systems: Landscape evolution. *Geomorphological Techniques*, 12, 1–24. <https://doi.org/10.13140/RG.2.1.1970.9047>
- van Dongen, R., Scherler, D., Wittmann, H., & von Blanckenburg, F. (2019). Cosmogenic ¹⁰Be in river sediment: Where grain size matters and why. *Earth Surface Dynamics*, 7(2), 393–410. <https://doi.org/10.5194/esurf-7-393-2019>
- van der Beek, P., & Bishop, P. (2003). Cenozoic river profile development in the upper Lachlan catchment (SE Australia) as a test quantitative fluvial incision models. *Journal of Geophysical Research*, 108(B6), 2309. <https://doi.org/10.1029/2002JB002125>
- Whipple, K. X. (2004). Bedrock rivers and the geomorphology of active orogens. *Annual Review of Earth and Planetary Sciences*, 32, 151–185. <https://doi.org/10.1146/annurev.earth.32.101802.120356>
- Whipple, K. X., Hancock, G. S., & Anderson, R. S. (2000). River incision into bedrock: Mechanics and relative efficacy of plucking, abrasion, and cavitation. *Geological Society of America Bulletin*, 112, 490–503. [https://doi.org/10.1130/0016-7606\(2000\)112<490:RIIBMA>2.0.CO;2](https://doi.org/10.1130/0016-7606(2000)112<490:RIIBMA>2.0.CO;2)
- Whipple, K. X., Snyder, N. P., & Dollenmayer, K. (2000). Rates and processes of bedrock incision by the upper Ukak River since the 1912 Novarupta ash flow in the Valley of Ten Thousand Smokes, Alaska. *Geology*, 28(9), 835–838. [https://doi.org/10.1130/0091-7613\(2000\)28<835:RAPOBI>2.0.CO;2](https://doi.org/10.1130/0091-7613(2000)28<835:RAPOBI>2.0.CO;2)
- Whipple, K. X., & Tucker, G. E. (1999). Dynamics of the stream-power river incision model: Implications for height limits of mountain ranges, landscape response timescales, and research needs. *Journal of Geophysical Research*, 104, 17,661–17,674. <https://doi.org/10.1029/1999JB900120>
- Whipple, K. X., & Tucker, G. E. (2002). Implications of sediment-flux-dependent river incision models for landscape evolution. *Journal of Geophysical Research*, 107(B2), 2002. <https://doi.org/10.1029/2000JB000044>
- Wickert, A. D., & Schildgen, T. F. (2019). Long-profile evolution of transport-limited gravel-bed rivers. *Earth Surface Dynamics*, 7(1), 17–43. <https://doi.org/10.5194/esurf-7-17-2019>
- Wilcock, P. R., & Crowe, J. C. (2003). Surface-based transport model for mixed-size sediment. *Journal of Hydraulic Engineering*, 129(2), 120–128. [https://doi.org/10.1061/\(ASCE\)0733-9429\(2003\)129:2\(120\)](https://doi.org/10.1061/(ASCE)0733-9429(2003)129:2(120))
- Wilcock, P. R., & Iverson, R. M. (2003). Prediction in geomorphology. In P. R. Wilcock, & R. M. Iverson (Eds.), *Prediction in geomorphology* (pp. 3–11). Washington, DC: American Geophysical Union (AGU). <https://doi.org/10.1029/135GM01>
- Willenbring, J. K., Codilean, A. T., & McElroy, B. (2013). Earth is (mostly) flat: Apportionment of the flux of continental sediment over millennial time scales. *Geology*, 41(3), 343–346. <https://doi.org/10.1130/G33918.1>
- Willgoose, G. R. (2005). Mathematical modeling of whole landscape evolution. *Annual Review of Earth and Planetary Sciences*, 33, 14.1–14.17. <https://doi.org/10.1146/annurev.earth.33.092203.122610>
- Willgoose, G. R. (2018). *Principles of soilscape and landscape evolution*. Cambridge: Cambridge University Press. <https://doi.org/10.1017/9781139029339>
- Willgoose, G. R., Bras, R. L., & Rodriguez-Iturbe, I. (1991a). A coupled channel network growth and hillslope evolution model: 1. Theory. *Water Resources Research*, 27(7), 1671–1684. <https://doi.org/10.1029/91WR00935>
- Willgoose, G. R., Bras, R. L., & Rodriguez-Iturbe, I. (1991b). A coupled channel network growth and hillslope evolution model: 2. Non-dimensionalization and applications. *Water Resources Research*, 27(7), 1685–1696. <https://doi.org/10.1029/91WR00936>
- Willgoose, G. R., & Hancock, G. R. (2011). Applications of long-term erosion and landscape evolution models. In R. P. C. Morgan, & M. A. Nearing (Eds.), *Handbook of erosion modelling*. John Wiley & Sons. <https://doi.org/10.1002/9781444328455.ch18>
- Willgoose, G. R., & Riley, S. R. (1998). Application of a catchment evolution model to predict the long-term erosion on the spoil heap at ranger uranium mine: Initial analysis. Supervising Scientist Report 132.
- Wilson, P. S., & Toumi, R. (2005). A fundamental probability distribution for heavy rainfall. *Geophysical Research Letters*, 32, L14812. <https://doi.org/10.1029/2005GL022465>
- Wilson, M., & Young, R. A. (2018). Phase 1 erosion studies: Study 1—Terrain analysis. West Valley Erosion Working Group. Retrieved from http://www.westvalleyphaseonestudies.org/Documents/EWG%20Final%20Study%201%20Report_Vol%201_2.21.18.pdf
- Wohl, E., & David, Gabrielle C. L. (2008). Consistency of scaling relations among bedrock and alluvial channels. *Journal of Geophysical Research*, 113, F04013. <https://doi.org/10.1029/2008JF000989>
- Wolman, M. G., & Miller, J. P. (1960). Magnitude and frequency of forces in geomorphic processes. *The Journal of Geology*, 68(1), 54–74.
- Wong, M., & Parker, G. (2006). Reanalysis and correction of bed-load relation of Meyer-Peter and Müller using their own database. *Journal of Hydraulic Engineering*, 132(11), 1159–1168. [https://doi.org/10.1061/\(ASCE\)0733-9429\(2006\)132:11\(1159\)](https://doi.org/10.1061/(ASCE)0733-9429(2006)132:11(1159))
- Yalin, M. S. (1992). *River mechanics*. Oxford: Pergamon. 220 p.
- Yanites, B. J., Tucker, G. E., Hsu, H.-L., Chen, C.-C., Chen, Y.-G., & Mueller, K. J. (2011). The influence of sediment cover variability on long-term river incision rates: An example from the Peikang River, central Taiwan. *Journal of Geophysical Research*, 116, F03016. <https://doi.org/10.1029/2010JF001933>
- Young, A. (1963). Deductive models of slope evolution. *Nachrichten der Akademie der Wissenschaften in Göttingen*, II(5), 45–66.